UDK/UDC: 621.791 **ISSN 0354-7965**

ZAVARIVANJE I ZAVARENE KONSTRUKCIJE

WELDING & WELDED STRUCTURES

God. 65	Br. 2	49-96	Beograd	Srbija	2020.
Vol. 65	No. 2	49-96	Belgrade	Serbia	2020.

ČASOPIS DRUŠTVA ZA UNAPREĐIVANJE ZAVARIVANJA U SRBIJI

SERBIAN WELDING SOCIETY QUARTERLY REVIEW

IZLAZI TROMESEČNO

CIP - Каталогизација у публикацији
Народна библиотека Србије, Београд

621.791

ZAVARIVANJE i zavarene konstrukcije : časopis Društva za unapređivanje zavarivanja u Srbiji = Welding & Welded Structures : Serbian Welding Society quarterly review / glavni i odgovorni urednik = editor-in-chief Milica Antić. – Vol. 41, no. 1 (1996)- . - Beograd : Društvo za unapređivanje zavarivanja u Srbiji, 1996-. (Beograd : VIS studio).-29 cm

Tromesečno.
ISSN 0354-7965 = Zavarivanje i zavarene konstrukcije
COBISS.SR-ID 105396743

CENE I NARUDŽBINA ZA 2020.

Cena pojedinačnog broja 825,00 dinara
Godišnja pretplata 2500,00 dinara
Tekući račun: 325-9500600002588-46

PRICE AND ORDER

Annual subscription: EUR 100
Account No. RS35325960160000041546
OTPVRS22 (VOJVOĐANSKA BANKA AD)
IBAN RS35325960160000041546

ŠTAMPA / PRINTED

"VIS STUDIO" d.o.o.
Aleksinačkih rudara 35, Beograd
Tiraž: 400 kom.

Časopis sufinansira Ministarstvo prosvete, nauke i tehnološkog razvoja Republike Srbije

Na osnovu mišljenja Ministarstva za nauku, tehnologije i razvoj Republike Srbije br. 413-00-2272/2001-01, časopis ZAVARIVANJE I ZAVARENE KONSTRUKCIJE je publikacija od posebnog interesa za nauku

2/2020

SADRŽAJ CONTENTS

Poštovani čitaoci,

Taman kada smo počeli da verujemo da ćemo nastaviti da živimo relativno normalno, ponovo se obrušio zagonentni virus i to još većom žestinom. Sve aktivnosti koje smo planirali za ovaj period, prinuđeni smo da pomerimo za neka, valjda bezbednija vremena.

Kao što obično biva da zlo ne dolazi samo, sredinom juna ove godine, izgubili smo člana našeg Upravnog odbora, Lazara Brestovačkog posle duge i teške bolesti. O našem Lazi više podataka u rubrici Vesti.

U ovom broju ćete imati prilike da se upoznate sa zanimljivim radovima izlaganim u okviru međunarodne konferencije „The 72 IIW Annual Assembly & International Conference“, July 2019, Bratislava, Slovačka.

U ovom trenutku najvažnije je da ostanete zdravi.

Uz želju da tako bude, do narednog susreta

Glavni i odgovorni urednik

Milica Antić, dipl.ing. CIWE, EWE

IN MEMORIAM

LAZAR BRESTOVAČKI, magistar tehničkih nauka

1965 – 2020.

Rođen u Novom Sadu, Mašinski fakultet-odsek proizvodni sistemi je završio u Novom Sadu a magistarski rad “Tehnologija zavarivanja nodularnog liva elektrolučnim postupcima u zaštitnom gasu” je odbranio na Fakultetu tehničkih nauka iz oblasti mašinstva-smer zavarivanje, livnički procesi i termička obrada u Novom Sadu.

Naše Društvo ostalo je bez još jednog pravog zaljubljenika u zavarivanje, kojem se predavao potpuno od edukatora do izvođača, od akademskog angažovanja do sopstvene firme, od unapred utabanih puteva do stranputica i novih istrajavanja.

Jedinstvenost našeg Laze kao da se sastojala upravo od poteza koje je vukao, ponekad iznenađujućih, vanserijskih i većinom uspešnih. Kada biste pomislili da mu je nešto izmaklo kontroli, postojao je njegov mir kojim je hrabrio sebe a nas očaravao.

Danas kad se preselio u besmrtnost, teško je poverovati da je uspeo da izgubi svoju najtežu bitku sa užasom neizlečive bolesti. Isto toliko je teško zamisliti i nastavak našeg rada bez njegove podrške i specifičnosti. Poslednja je prilika da se zahvalimo na tome.

Neka mu je večna slava.

Michael Regev[1] [a], Stefano Spigarelli[2] [b]

Microstructural processes occurring during creep of friction stir welded AA2024-T3 alloy
Mikrostrukturni procesi koji se odvijaju tokom puzanja legure AA2024- T3 zavarene trenjem sa mešanjem

Originalni naučni rad / Original scientific paper
Rad je u izvornom obliku objavljen u okviru 72. IIW godišnje Skupštine i međunarodne konferencije održane u Bratislavi-Slovačka 07-12. Jula 2019
Rad primljen / Paper received:
Maj 2020.

Adresa autora / Author's address:
[1]Mechanical Engineering, ORT Braude College of Engineering, Karmiel, Israel
[2]Dipartimento di Meccanica, Università Politecnica delle Marche, Ancona, Italy
[a]michaelr@braude .ac.il, [b]s.spigarelli@staff .univpm.it

Ključne reči: Zavarivanje trenjem sa mešanjem, Aluminijumske legure 2024, taloženje, dinamička rekristalizacija

Keywords: friction stir welding, aluminum alloys, 2024, precipitation, dynamic recrystallization

Abstract
The poor weldability of AA2024 aluminum alloy limits its use for industrial applications. Being a non-fusion welding process, Friction Stir Welding (FSW) seems to be a promising solution for welding this alloy. FSW was applied in the current study in order to butt weld AA2024-T3 aluminum alloy plates and to study the creep behavior of the weld. Creep tests were conducted at 250 ^{0}C and 315 ^{0}C both on the parent material and on the friction stir welded specimens. A comprehensive Transmission Electron Microscopy (TEM) study together with High Resolution Scanning Electron Microscopy (HRSEM) study and Energy Dispersive X-ray Spectroscopy (EDS) analysis were conducted in order to investigate the microstructural processes. The parent material seems to contain two kinds of Cu-rich precipitates - coarse precipitates having the size of a few microns each and uniformly dispersed fine nanosized precipitates. However, this microstructure was found to be unstable at the temperature range of 250-315 ^{0}C, secondary precipitation was found to take place, this secondary precipitation is responsible for grain boundary decoration and the appearance of secondary rod-shaped precipitates and for some degree of coarsening of the nanosized precipitates inside the grains. TEM study yielded that the material undergoes dynamic recrystallization (DRX) during creep as well as during the FSW process. Various stages of the development of dislocation networks into a cellular dislocation structure and finally into dislocation free recrystallized grains were recorded. The friction stir welded material, which has already recrystallized during welding, undergoes DRX during creep so that ultra-fine grains are being created concurrently. Precipitation processes at the friction

Rezime
Loša zavarljivost aluminijumske legure AA2024 ograničava njihovu upotrebu u industrijskim primenama. Čini se da je postupak zavarivanja bez topljenja, trenjem sa mešanjem (FSW) obećavajuće rešenje za zavarivanje ove legure. FSW je primenjen u ovoj studiji za zavarivanje ploče od aluminijumske legure AA2024-T3 i kako bi se proučilo puzanje šava. Ispitivanja puzanja su obavljena na 250 ^{0}C i 315 ^{0}C, na osnovnom materijalu i na epruvetama zavarenim trenjem sa mešanjem. Sveobuhvatna transmisiona elektronska mikroskopija (TEM) zajedno sa skeniranjem elektronskim mikroskopom visoke rezolucije (HRSEM) i analizom rendgenske spektroskopije sa energetskom disperzijom (EDS) sprovedene su u cilju ispitivanja mikrostrukturnih procesa. Čini se da osnovni materijal sadrži dve vrste taloga koji sadrže Cu - grubi talozi veličine nekoliko mikrona i jednoliko dispergovane sitne taloge nanoveličine. Međutim, za ovu mikrostrukturu je utvrđeno da je nestabilna u temperaturnom opsegu od 250 do 315^{0}C, postojali su sekundarni talozi, ovi sekundarni talozi su odgovorni za dekoraciju granica zrna i pojavu sekundarnih taloga u obliku štapa i za određeni stepen ogrubljenja taloga nanoveličine u zrnu. TEM je pokazao da se materijal podvrgava dinamičkoj rekristalizaciji (DRX) tokom puzanja, kao i tokom FSW procesa. Zabeležene su različite faze razvoja dislokacionih mreža u ćelijsku dislokacionu strukturu i konačno u rekristalizovana zrna bez dislokacija. Materijal zavaren trenjem sa mešanjem koji se već rekristalizirao tokom zavarivanja, podvrgnut je DRX-u tokom puzanja,

stir welded material occur as well during creep. The instability of the microstructure during creep and exposure to high temperature plays an important role in the analysis of the creep results. The influence of the above microstructure changes occurring during creep on the creep behavior will be referred and discussed.

1. Introduction

The 2024 (Al-4%Cu-1.5%Mg) aluminum alloy is one of the most widely used materials for airplane structures [1-3], and as such has been investigated in depth to clarify the relationships between its microstructure and its mechanical properties. Although Al-Cu-Mg alloys cannot be considered new materials since their early applications date back to World War I, the 2024 is still the reference material for aerospace and has continuously been improved, with Ag addition to its composition being only one of the most recent developments [4,5]. The creep response of the 2024 alloy has been investigated in detail, with one of the first studies dating back to the late 1950s [6]. More recently, the same alloy was the subject of detailed mechanical and microstructural investigations aimed at correlating the microstructure evolution and the creep response [7-9]. Although at first glance one could legitimately conclude that this material is now fully characterized, many researchers continue to investigate its high temperature response [10-13]. The precipitate study of AA2024 continues to this day. Among other publications dealing with precipitation study, Wang and Starink [14] and Zhang et al. [l 5] reported new characterized precipitates. Researchers seem to agree that two aging sequences take place. The first is the aging sequence:

$$\alpha(ssss) \rightarrow GP\ zones \rightarrow \theta''(Al_3Cu) \rightarrow$$
8' SAI Cir) —r 8 SAI Cir)

while the second is the S aging sequence:

a ssss) —r GP B zones —r S " SAI CRM g) —r
S' {Al CUM p) —r S {Al CUM p)

Both sequences begin with a Super Saturated Solid Solution (SSSS) and end with stable precipitates.

tako da se istovremeno stvaraju ultra-fina zrna. Proces taloženja na materijalu koji je zavaren trenjem sa mešanjem, odvija se i tokom puzanja. Nestabilnost mikrostrukture tokom puzanja i izloženost visokoj temperaturi igra važnu ulogu u analizi rezultata puzanja. Uticaj gore navedenih promena mikrostrukture koje nastaju tokom puzanja biće prikazan i razmatran.

1. Uvod

Aluminijska legura 2024 (Al-4% Cu-1,5% Mg) jedan je od najčešće korišćenih materijala za avionske konstrukcije [1-3], i kao takva je detaljno istražena kako bi se razjasnila veza između njene mikrostrukture i mehaničkih svojstava. Iako se legure Al-Cu-Mg ne mogu smatrati novim materijalima, jer njihova rana primena datira još iz Prvog svetskog rata, legura 2024 je još uvek referentni materijal za vazduhoplovstvo i kontinuirano se unapređuje, uz dodatak Ag u njen sastav samo jedan od najvažnijih nedavnih dešavanja [4,5].

Odgovor legura 2024 na puzanje detaljno je istražen, a jedno od prvih istraživanja datira iz kasnih 1950-ih [6]. U novije vreme, ista legura je bila predmet detaljnih mehaničkih i mikrostrukturnih istraživanja usmerenih na povezanost razvoja mikrostrukture i puzanja [7-9]. Iako se na prvi pogled s pravom može zaključiti da je ovaj materijal u potpunosti okarakterisan, mnogi istraživači nastavljaju da istražuju njegovo ponašanje na visokim temperaturama [10-13]. Studija o taloženju AA2024 nastavlja se do danas. Između ostalih publikacija koje se bave proučavanjem taloga, Vang i Starink [14] i Zhang i dr. [l 5] izvestio je o novim karakterističnim talozima. Čini se da se istraživači slažu sa tim da se odvijaju dve sekvence starenja. Prva sekvenca starenja Θ je:

$$\alpha(ssss) \rightarrow GP\ zones \rightarrow \theta''(Al_3Cu) \rightarrow$$
8' SAI Cir) —r 8 SAI Cir)

dok je druga sekvenca starenja S

a ssss) —r GP B zones —r S " SAI CRM g) —r
S' {Al CUM p) —r S {Al CUM p)

Obe sekvence počinju super zasićenim čvrstim rastvorom (SSSS) i završavaju se stabilnim talozima.

The poor weldability of the 2024 aluminum alloy using arc welding processes limits the use of the material for industrial applications. Friction Stir Welding (FSW), on the other hand, seems to be a promising solution for welding this alloy. Several studies have used Transmission Electron Microscopy (TEM) to investigate the microstructural changes occurring during FSW of 2024 [16-21]. Leal and Loureiro [16] conducted a dislocation study on friction stir welded 6063-T6 aluminum alloy and reported on the formation of a cellular structure at the nugget zone as opposed to the Thermo Mechanically Affected Zone (TMAZ). While they studied 6063-T6 aluminum alloy, their work is nevertheless mentioned here due to the importance of their TEM study of the Al matrix. Fu et al. [17] investigated the effect of different heat input conditions on grain size during FSW of 2024-T3 aluminum alloy. They reported on dynamic recrystallization (DRX) and subgrain formation at relatively low heat inputs and on extensive grain growth at higher heat inputs. Chen et al. [18] came to the same conclusion regarding grain size. They also pointed to the dissolution of the strengthening precipitates at high welding heat input together with re-precipitation. Dixit et al. [19] referred to precipitation of S (AlzCuMg) phase precipitates together with the formation of dislocation structures, subgrains and the occurrence of recrystallization processes within the nugget zone. Jones et al. [20] reported on fine equiaxed grains (4-5 μm) at the nugget zone, with some containing high dislocation density while others appearing to have low densities. The grains of the nugget were found to contain two types of precipitates fine scale S precipitates and larger f2 (Al2Cu) precipitates. Genevois et al. [21] identified three different dislocation structures: The Heat Affected Zone (HAZ) close to the base metal was characterized by dislocation density similar to that of the base metal, while at the HAZ close to the TMAZ the dislocation density was found to be relatively high, similar to that of the TMAZ in which a network structure was observed. In the nugget, where deformation during welding was maximal, few dislocations remained after welding due to DRX.

In summary, different researchers seem to agree that DRX occurs during friction stir welding of AA2024-T3. The current paper examines the creep of a complex microstructure that underwent extensive plastic deformation, in turn yielding recrystallization prior to creep (during welding). In addition, the AA2024-T3 is known to undergo different precipitation and aging stages. To the best knowledge of the authors, no model for creep of

Loša zavarljivost aluminijumske legure 2024 elektrolučnim postupcima zavarivanja ograničava upotrebu materijala za industrijske namene. Čini se da je zavarivanje trenjem sa mešanjem (FSW) obećavajuće rešenje za zavarivanje ove legure. Nekoliko studija koristi transmisionu elektronsku mikroskopiju (TEM) za istraživanje mikrostrukturnih promena koje su se dogodile tokom FSW legure 2024 [16-21]. Leal i Loureiro [16] sproveli su dislokacijsku studiju na aluminijskoj leguri 6063-T6 zavarenoj trenjem sa mešanjem i izvestili o formiranju ćelijske strukture u zoni gromuljice, za razliku od termo mehanički zahvaćene zone (TMAZ). Dok su proučavali leguru aluminijuma 6063-T6, njihov rad se ovde ipak spominje zbog važnosti njihove TEM studije Al matrice. Fu i dr. [17] istražio je uticaj različitih uslova toplote na veličinu zrna tokom FSW aluminijumske legure 2024-T3. Izveštavali su o dinamičkoj rekristalizaciji (DRX) i stvaranju subzrna pri relativno malim unosima toplote i o ekstenzivnom rastu zrna pri većim unosima toplote. Chen i dr. [18] došli su do istog zaključka u pogledu veličine zrna. Takođe su ukazali na rastvaranje taloga za ojačanje pri visokom unosu toplote pri zavarivanju, zajedno sa ponovnim taloženjem. Dikit i dr. [19] saopštavaju o taloženju taloga S (AlzCuMg) faze zajedno sa formiranjem dislokacionih struktura, subzrna i pojavom procesa rekristalizacije u zoni izrasline. Jones i dr. [20] izveštavali su o finim istoosnim zrncima (4-5 μm) u zoni izrasline, pri čemu neki imaju veliku gustinu dislokacija, dok drugi izgleda da imaju malu gustinu. Otkriveno je da zrno u izbočini sadrži dve vrste taloga; sitnih taloga S i više f2 (Al2Cu) taloga. Genevois i dr. [21] identifikovali su tri različite dislokacione strukture: Zona uticaja toplotne energije (HAZ) blizu osnovnog metala bila je okarakterisana gustinom dislokacije sličnom kao kod osnovnog metala, dok je kod HAZ-a blizu TMAZ-a gustina dislokacija relativno visoka, slično kao kod TMAZ-a u kome je primećena mrežna struktura. U izbočini, gde je deformacija tokom zavarivanja bila maksimalna, nakon zavarivanja zbog DRX ostalo je nekoliko dislokacija.

Ukratko, čini se da se različiti istraživači slažu da se DRX javlja tokom zavarivanja trenjem sa mešanjem legure AA2024-T3. Sadašnji rad ispituje puzanje složene mikrostrukture koja je pretrpela veliku plastičnu deformaciju, zauzvrat dajući rekristalizaciju pre puzanja (tokom zavarivanja). Pored toga, poznato je da AA2024-T3 prolazi kroz različite faze taloženja i starenja. Koliko je poznato

such a complex microstructure has ever been proposed.

2. Experimental procedure

The material used for this study was commercial AA2024- T3 aluminum alloy in the form of 200 mm xl00 mm plates, 3.175 mm thick. The above plates were butt welded to each other using a SHARNOA CNC milling machine. The simple H-13 steel welding tool used consisted of a pin of 4.5 mm diameter, 3 mm height and a 20 mm diameter shoulder.

All the welded specimens were visually examined. Metallographic specimens were extracted from the welds characterized by proper morphology. Four metallographic specimens were prepared from each of them. The first metallographic specimen was taken from the first quarter of the seam, the second from the second quarter and so on, in order to detect inner porosity or cracking. The welds found to be of the highest quality based on metallographic cross- sections were then radiographically checked. The optimal welding parameters were found to be a rotational speed of 800 rpm and a transverse speed of 80 mm/min. The metallographic study was conducted using a Zeiss AXl0 optical microscope and a Zeiss Ultra Plus High Resolution Scanning Electron Microscope (HRSEM).

The configuration of the creep specimens with respect to the welded specimen is shown in figure la, while its dimensions are given in Fig. lb. The gage length was 25 mm, with the center of the weld seam corresponding to the center of the creep specimen. Note that the gage length included the weld nugget, the TMAZs, the HAZs and the parent materials on both sides of the weld.

autorima, nikada nije predložen model za puzanje tako složene mikrostrukture.

2. Eksperimentalni postupak

Materijal korišćen za ovu studiju je komercijalna legura aluminija AA2024-T3 u obliku ploča od 200 x l00 mm, debljine 3.175 mm. Gore navedene ploče su međusobno zavarene pomoću glodalice SHARNOA CNC. Jednostavan alat za zavarivanje od čelika H-13 sastojao se od igle prečnika 4,5 mm, visine 3 mm i prečnika držača od 20 mm.

Svi zavareni uzorci su vizuelno pregledani. Metalografski uzorci su uzeti iz šavova koje karakteriše odgovarajuća morfologija. Iz svakog od njih pripremljena su četiri metalografska uzorka. Prvi metalografski uzorak uzet je iz prve četvrtine šava, drugi iz druge četvrtine i tako dalje, da bi se otkrila unutrašnja poroznost ili prslina. Pronađeni su najkvalitetniji zavari na osnovu metalografskih preseka, a zatim su radiografski pregledani. Otkriveni su optimalni parametri zavarivanja, brzina rotacije od 800 o/min i poprečna brzina od 80 mm/min. Metalografska studija izvedena je uz pomoć optičkog mikroskopa Zeiss AKSl0 i Zeiss Ultra Plus skenirajućeg elektronskog mikroskopa (HRSEM).

Konfiguracija uzoraka za puzanje u odnosu na zavarene epruvete prikazana je na slici la, dok su njene dimenzije date na slici lb. Dužina merenja je 25 mm, a sredina zavarenog šava odgovara sredini uzorka puzanja. Imajte na umu da je dužina merača obuhvatala izbočinu, TMAZ-ove, HAZ-ove i osnovni materijal sa obe strane šava.

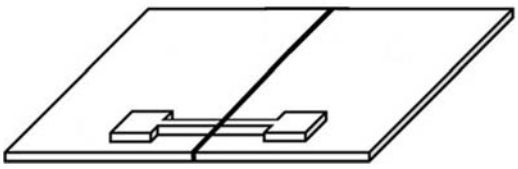

(a)

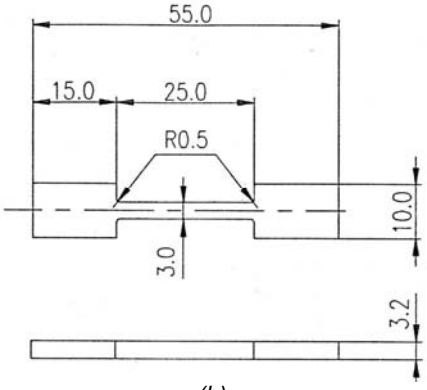

(b)

Fig. 1 *Creep specimen (a) Configuration; (b) A drawing*
Sl.1. *Epruveta za puzanje (a) konfiguracija (b) crtež*

Constant load creep tests were conducted on the base alloy (CLb) and on the cross-welds (CLcw) at 250^{0}C and at 3l5°C, in most cases up to fracture. The experimental temperature, which was well above the maximum allowable temperature usually prescribed for the 2024 alloy, was specifically chosen to facilitate studying the effects of microstructural instability on the creep response. To achieve the same goal, additional variable load experiments were carried out on the base alloy (CLcw). In these experiments, the initial stress (25 MPa, except in one experiment in which the initial stress was 15 MPa) was maintained until the minimum creep rate range was attained. The test duration required to reach the minimum creep rate range was estimated based on the results of CLb, which had previously been carried out under the corresponding stress. The applied stress was then abruptly increased and maintained up to specimen rupture. The gage-length of the cross-weld specimens was marked by micro- hardness indentations distanced lmm from one another. After creep, the distance between the indentations was measured to evaluate the strain distribution along the specimen.

TEM investigation was conducted by using an FEI Tecnai G° T20 TEM. The specimens for the TEM study were taken from the neck of the broken creep specimens, as close as possible to the fracture surface.

The thermal stability of the microstructure was studied by means of aging experiments conducted at 300'C for up to 280 hours.

3. Results

Fig. 2 shows an optical micrograph of the parent AA2024- T3 taken parallel to the rolling direction. In the figure, the grains are elongated due to the rolling process.

Ispitivanja puzanja konstantnim opterećenjem izvedena su na osnovnoj leguri (CLb) i na poprečnim zavarima (CLcv) na 250^{0}C i na 3l5 ° C, u većini slučajeva do loma. Eksperimentalna temperatura, koja je bila znatno iznad maksimalne dozvoljene temperature, obično propisane za leguru 2024, posebno je odabrana da olakša proučavanje efekata mikrostrukturne nestabilnosti na reakciju na puzanje. Da bi se postigao isti cilj, obavljeni su dodatni eksperimenti sa promenljivim opterećenjem na osnovnoj leguri (CLcv). U tim eksperimentima je inicijalni napon (25 MPa, osim u jednom eksperimentu u kome je početni napon bio 15 MPa) održavan sve dok se nije dostigao raspon minimalne brzine puzanja. Trajanje testa potrebno da se dostigne raspon minimalne brzine puzanja procenjeno je na osnovu rezultata CLb, koji su prethodno izvedeni pod odgovarajućim naponom. Primenjeni napon je naglo porastao i održavao se sve do pucanja uzorka. Debljina dužine ukrštenih uzoraka bila je obeležena udubljenjima mikrotvrdoće udaljenim mm od jednog do drugog. Nakon puzanja, izmerena je udaljenost između udubljenja kako bi se procenila raspodela naprezanja po uzorku.

TEM istraživanje je sprovedeno korišćenjem FEI Tecnai G ° T20 TEM. Uzorci za TEM ispitivanje uzeti su sa vrata slomljenih uzoraka, što bliže površini preloma.

Termička stabilnost mikrostrukture proučavana je eksperimentima starenja vođenim na 300 ° C tokom 280 sati.

3. Rezultati

Sl. 2 prikazuje optičku mikrografiju osnovne legure AA2024-T3 uzete paralelno sa pravcem valjanja. Na slici su zrna izdužena zbog procesa valjanja.

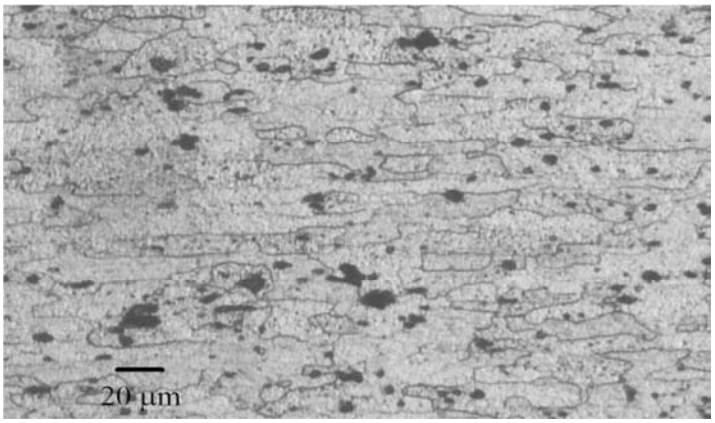

Fig. 2 *An optical micrograph of the parent AA2024-T3*
Sl.2. *Optička mikrografija osnovnog materijala A2024-T3*

Fig. 3 shows an optical micrograph taken from the nugget zone. In contrast to the elongated grains in figure 2, the grains seen in figure 3 are equi-axed and their average size is a few microns each.

Sl. 3 prikazuje optičku mikrografiju snimljenu u zoni izbočine. Za razliku od izduženih zrnaca na slici 2, zrna prikazana na slici 3 su jednosmerna i njihova prosečna veličina je nekoliko mikrona

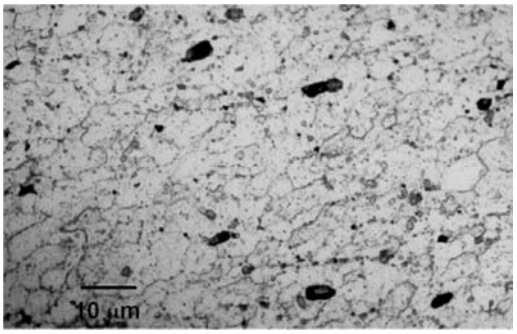

Fig. 3 *An optical micrograph of the nugget zone of friction stir welded AA2024-T3*
Sl.3. *Optička mikrografija izbočene zone FSW AA2024-T3*

Micro hardness tests showed that the hardness of the material as received was 100-110 HV. Despite the grain refinement, the FSW process caused only a moderate increase in hardness, which reached its maximum values (130 HV) at the center of the nugget zone and dropped down to 95-100 HV, i.e., to values slightly lower than the base metal, in the heat affected zones.

Figure 4 shows the dependence of the minimum creep rate on the applied stress for the CLb, VLb and CLcw experiments. The CLb results lie along a straight line with a slope of 4.4. In contrast, the slope of the curve of the VLb experiments is substantially higher than 4.4. Fig. 4 also plots the minimum creep rate of the cross weld samples after FSW. The figure clearly shows that the FSW samples exhibited a minimum creep rate that is higher by orders of magnitude than that of the base alloy, tested either under constant or variable load.

Testovi mikro tvrdoće pokazali su da je tvrdoća materijala koji je primljene 100-110 HV. I pored rafinacije zrna, FS>W proces je izazvao samo umereno povećanje tvrdoće koja je dostigla svoje maksimalne vrednosti (130 HV) u središtu izbočene zone i spustila se do 95-100 HV, tj. vrednosti nešto niže od osnovnog materijala, u zonama pod uticajem toplote.

Slika 4 prikazuje zavisnost minimalne brzine puzanja o primenjenom stresu za CLb, VLb i CLcv eksperimente. Rezultati CLb leže duž ravne linije sa nagibom od 4,4. Suprotno tome, nagib krivulje VLb eksperimenata znatno je veći od 4,4. Sl. 4 takođe prikazuje minimalnu brzinu puzanja uzoraka unakrsnog zavarivanja nakon FSV. Na slici je jasno vidljivo da su uzorci FSV pokazali najmanju brzinu puzanja koja je veća za redosled veličine od stope osnovne legure, testirane ili pod konstantnim ili promenljivim opterećenjem.

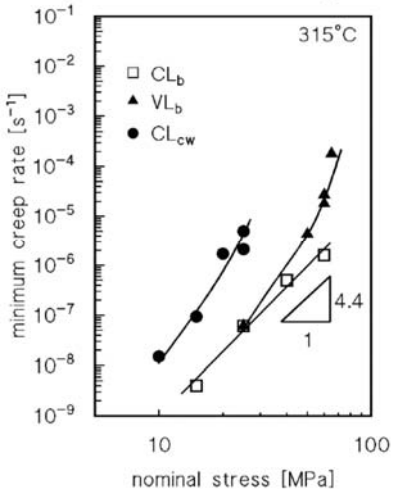

Fig. 4 *The minimum creep rate as a function of the nominal testing stress for the base alloy and for the cross-welded FSW samples*
Sl. 4 *Minimalna brzina puzanja kao funkcija nominalnog ispitnog naprezanja za baznu leguru i za poprečno zavarene FSW uzorke*

Fig. 5 shows two creep curves of friction stir welded specimens. Curve (a) refers to a test carried out at 3150C under 15MPa. This test was continued until rupture. Curve (b) refers to a test carried out at 315 ^{0}C under 20 MPa, which was interrupted when the minimum creep rate was reached, prior to the tertiary stage.

Sl. 5 prikazuje dve krivine puzanja uzoraka zavarivanih trenjem pomoću mešavina trenja. Krivulja (a) se odnosi na test sproveden na 3150C ispod 15MPa. Ovaj test je nastavljen do puknuća. Kriva (b) odnosi se na test sproveden na 315 ^{0}C ispod 20 MPa, koji je prekinut kada je dostignuta minimalna brzina puzanja, pre tercijarne faze.

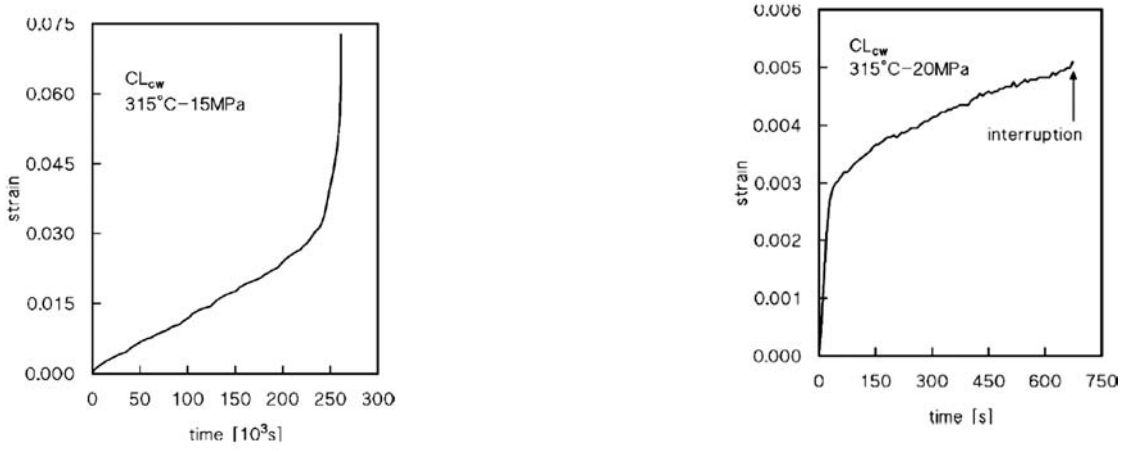

a) b)

Fig. 5 *Creep curves for tests carried out on cross-weld FSW samples (a) Until rupture; (b) Interrupted*
Sl. 5 *Krive puzanja za ispitivanja izvedena na uzorcima unakrsnog zavarivanja FSW (a) Do prekida; (b) Prekinuto*

Fig. 6 shows an optical micrograph of the creep specimen after the test was intemipted. An extended 1.4 mm long crack clearly appears at the weld root. Similar cracks were found in all the FSW crept samples. Micro-hardness indentations created on the creep specimen prior to the test at a constant spacing of 1 mm showed that most of the gage length deformation occurred at a 2 mm long interval in the vicinity of the crack. This led to the conclusion that rupture was accompanied by extensive localized deformation.

Sl. 6 prikazuje optičku mikrografiju uzorka za puzanje nakon što se test pokrenuo. Proširena pukotina dužine 1,4 mm jasno se pojavljuje na korenu zavara. Slične prsline pronađene su u svim uzorcima FSW, podvrgnutim starenju. Udubljenja mikro tvrdoće stvorena na uzorku za puzanje, pre ispitivanja, pri konstantnom razmaku od 1 mm pokazala su da se najveći deo deformacije merača dogodio u razmaku od 2 mm u blizini prsline. To je dovelo do zaključka da je lom praćen obimnom lokaliziovanom deformacijom.

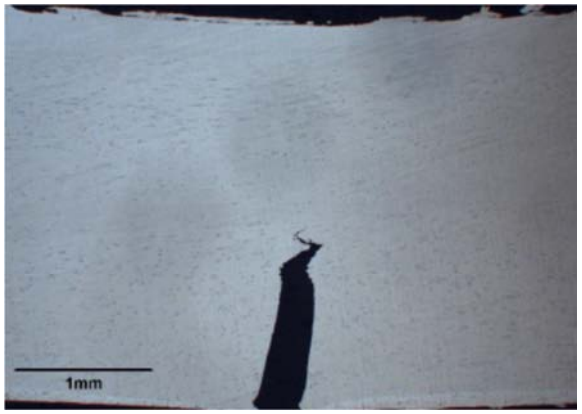

Fig. 6 *An optical micrograph of the creep specimen after interruption (25 MPa, 315 C)*
Fig. 6 An optical micrograph of the creep specimen after interruption (25 MPa, 315 C)

A Bright Field (BF) TEM micrograph of AA2024-T3 parent material taken near <001> Z.A is shown in figure 7, while a selected area electron diffraction pattern of <00l > Z.A is given in Fig. 7b. A sub-grain structure whose boundaries consist of dislocation networks can be clearly identified in this micrograph. Moreover, as known, when a crystal is tilted into a certain zone axis, its bright field becomes darker because more energy goes to the diffracted beams instead of to the incident beam. Here the dark contrast proves that all three are near <001> Z.A., as can be expected in the case of sub-grains as opposed to grains. The size of these sub-grains is a few microns each.

Na slici 7 prikazana je TEM mikrografija osnovnog materijala AA2024-T3 sa svetlim poljem (BF),, dok je odabrani dijagram difrakcije elektrona od <00l > Z.A dat na slici 7b. Sstruktura subzrna čije se granice sastoje od dislokacijskih mreža može se jasno identifikovati u ovoj mikrografiji. Štaviše, kao što je poznato, kad se kristal nagne u određenu zonu ose, njegovo svetlo polje postaje tamnije jer više energije odlazi na difraktovane zrake, umesto na padajući snop. Ovde tamni kontrast dokazuje da su sva tri blizu <001> Z.A., kao što se može očekivati u slučaju subzrna, za razliku od zrna. Veličina ovih subzrna je nekoliko mikrona.

a) b)

Fig.7 *(a) BF TEM micrograph of AA2024-T3 parent material taken near <001> Z.A.; (b) Selected area electron diffraction pattern of <001> Z.A*

Sl. 7 *(a) BF TEM mikrografija osnovnog materijala AA2024-T3 snimljena blizu <001> Z.A .; (b) Odabrani elektronski difrakcijski oblik <001> Z.A*

Fig. 8a shows a BF TEM micrograph of AA2024-T3 after creeping 17 hrs at 250 ^{0}C under l20MPa taken near <011> Z.A., while a selected area electron diffraction pattern of <011> Z.A is shown in Fig. 8b. The dislocation networks seen in figure 7 are not discernible in figure 8. The dark contrast of the grains tilted to <01l > Z.A makes it possible to identify them and to estimate their size. It seems that there are many submicron grains, and the appearance of such ultrafine single grains can be related to DRX. Note that the sub-grain structure almost disappeared.

Sl. 8a prikazuje BF TEM mikrografiju AA2024-T3 nakon puzanja 17 sati na 250 ° C pod l20MPa snimljenom blizu <011 Z.A., dok je odabrani difrakcijski elektronski obrazac <011> Z.A prikazan na slici 8b. Mreže dislokacije prikazane na slici 7 nisu prepoznatljive na slici 8. Tamni kontrast zrna nagnutog ka <01l > Z A omogućava da se identifikuje i proceni njihova veličina. Čini se da postoji mnogo subzrna , a pojava takvih ultrafinih pojedinačnih zrna može biti povezana sa DRX-om. Treba zapaziti da da je struktura subzrna gotovo nestala.

a) b)

Fig. 8 (a) BF TEM micrograph of AA2024-T3 after creeping 17 hrs at 250°C under 120MPa taken near <011> Z.A.; (b) Selected area electron diffraction pattern of <011> Z.A

Sl. 8 (a) BF TEM mikrografija AA2024-T3 posle puzanja 17 sati na 250 ° C pod 120MPa, snimljena blizu <011> Z.A .; (b) Izabrani elektronski difrakcijski oblik <011> Z.A

Fig. 9 depict BF TEM micrographs of the friction stir welded AA2024-T3 in its as-weld condition. No evidence of sub-grain structure was detected. For example, Fig. 9a was taken after tilting the right grain to <001> Z.A. Its selected area electron diffraction pattern is shown in Fig. 9b. Tilting the left grain to <00l > Z.A. (Fig. 9d) required a large tilt angle. This shows, in turn, that these are two different grains, each a few microns in size.

Sl. 9 prikazuju BF TEM mikrografije AA2024-T3 zavarenog trenjem sa mešanjem, u stanju zavarivanja. Nisu otkriveni dokazi o strukturi subzrna. Na primer, slika 9a je uzeta nakon nagiba desnog zrna do <001> Z.A. Njegov odabrani oblik difrakcije elektrona za to područje prikazan je na slici 9b. Naginjanje levog zrna do <00l> Z.A. (Sl. 9d) zahteva veliki ugao nagiba. To pokazuje, sa svoje strane, da su to dva različita zrna, svaka veličine nekoliko mikrona.

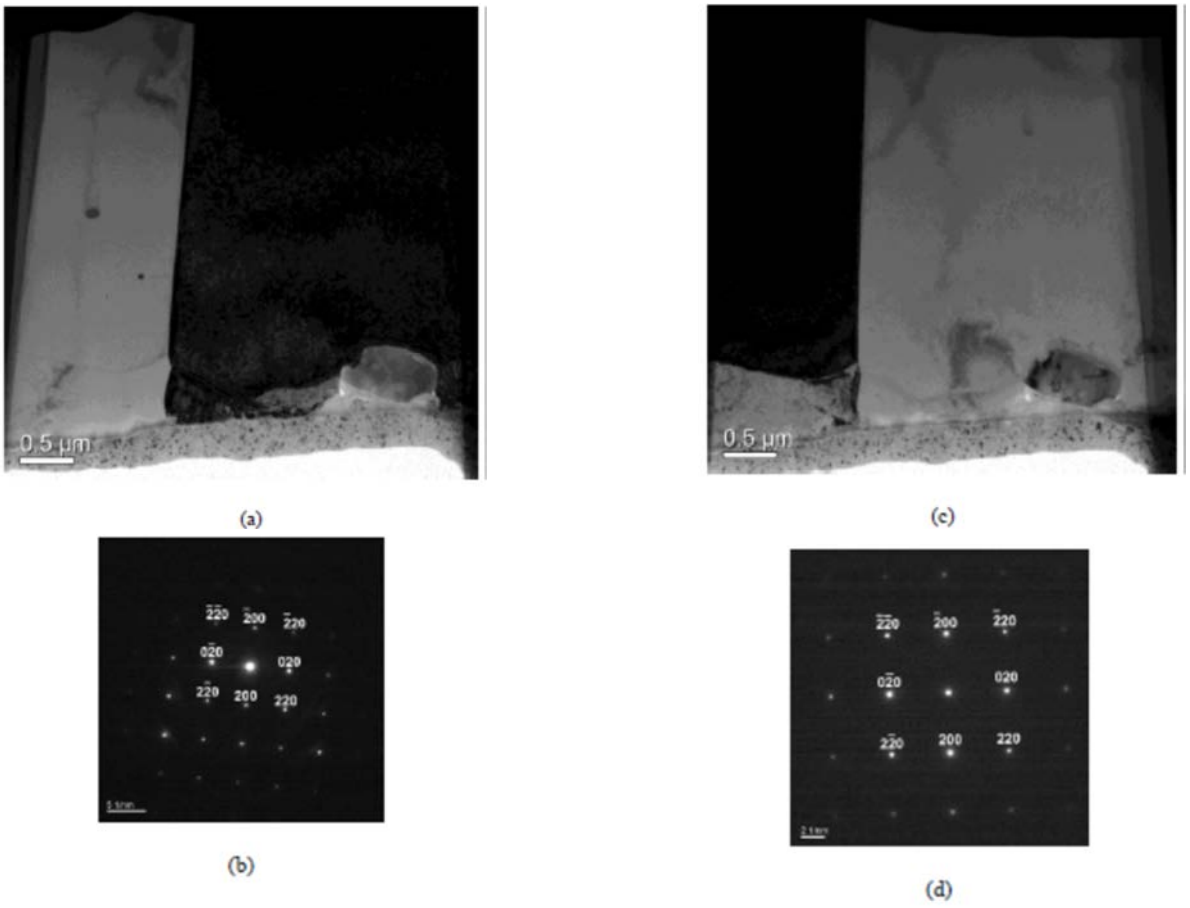

Fig. 9 *(a, c) BF TEM micrograph of friction stir welded AA2024- T3 taken while the dark grains were tilted to <001> Z.A.; (b,d) Selected area electron diffraction patterns of <001> Z.A taken from each grain*
Sl. 9 *(a, c) BF TEM mikrografija AA2024-T3 zavarenog trenjem sa mešanjem, snimljena dok su tamna zrna nagnuta ka <001> Z.A .; (b, d) Izabrani uzorci elektronske difrakcije elektrona <001> Z.A uzeti iz svakog zrna*

Figure 10a shows a BF TEM micrograph of friction stir welded AA2024-T3 after creeping 139 hrs at 3150C under l20MPa. The dark grain was tilted to <013> Z.A. Its selected area electron diffraction pattern is shown in Fig. 10b, while the selected area electron diffraction pattern of the neighboring grain on its right is depicted in Fig.10c.
It can be concluded that these are two separate grains, each a few microns in size. Finer grains can be seen in Fig. 10a as well.

Na slici 10a prikazana je BF TEM mikrografija AA2024-T3 zavarenog trenjem sa mešanjem, nakon puzanja 139 sati na 315 ° C pod l20MPa. Tamno zrno je nagnuto ka <013> Z.A. Njegov odabrani oblik područja difrakcije elektrona prikazan je na slici 10b, dok je odabrani dijagram difrakcije elektrona susednog zrna sa desne strane prikazan na slici 10c.
Može se zaključiti da su to dva odvojena zrna, svaka veličine nekoliko mikrona. Finija zrna mogu se videti i na slici 10a.

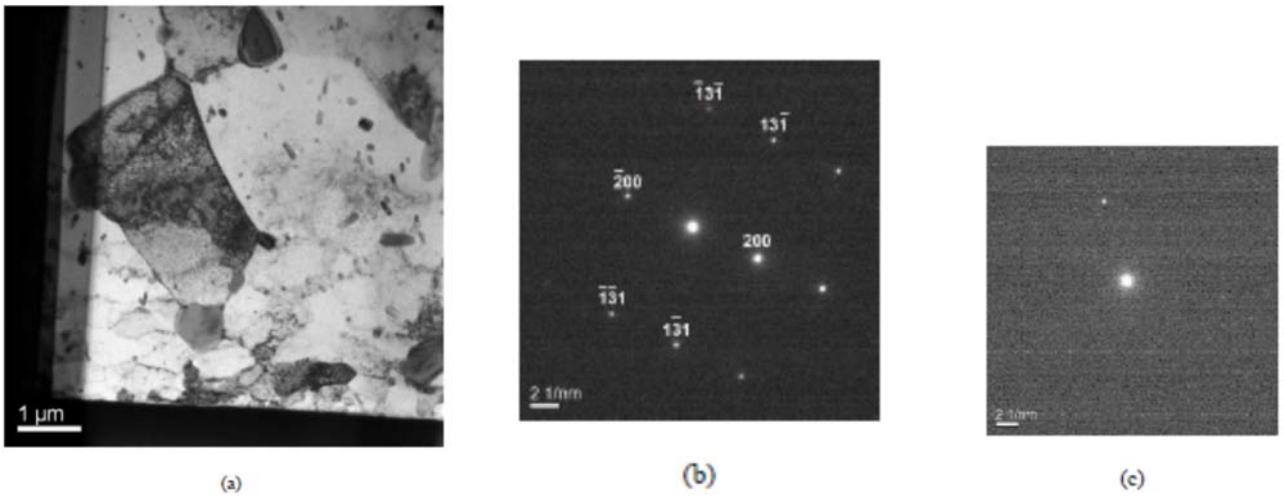

Fig. 10 *(a) BF TEM micrograph of friction stir welded AA2024-T3 after creeping 139 hrs at 315^C; (b) Selected area electron diffraction pattern of <013> Z.A — dark grain; (c) Selected area electron diffraction pattern taken from the neighboring grain*

Sl. 10 *(a) BF TEM mikrografija AA2024-T3 zavarenog trenjem sa mešanjem, nakon puzanja 139 sati na 315 ° C; (b) Odabrani oblik difrakcije elektrona <013> Z.A - tamno zrno; (c) Odabrani dijagram difrakcije elektrona odabranog područja iz susjednog zrna*

Fig. 11 shows two HRSEM images. Fig. 11a refers to the as-received parent metal, while figure 11 b was taken after 170 hours of exposure to 315 ^{0}C. Coarse precipitates a few microns in size are discernible in the as-received material, together with evenly dispersed nano-sized precipitates. The aged material (Fig. 11b) reveals two other types of precipitates. The first type of precipitates decorates the grain boundaries, while the second type contains platelet-like or rod-shaped precipitates. Coarsening to some degree of the nano-sized precipitates inside the grains can be seen as well.

Sl. 11 prikazuje dve HRSEM slike. Sl. 11a odnosi se na osnovni metal u isporučenom stanju, dok je slika 11b uzeta nakon 170 sati izloženosti na 315 ^{0}C. Grubi talozi veličine nekoliko mikrona mogu se primetiti po primljenom materijalu, zajedno sa ravnomerno dispergovanim talogom nano veličine. Stareni materijal (Sl. 11b) otkriva dve druge vrste taloga. Prva vrsta taloga dekoriše granice zrna, dok druga vrsta sadrži u obliku trombocita ili šipke. Takođe se može videti grubo izlučeni talog nano veličine u zrnu.

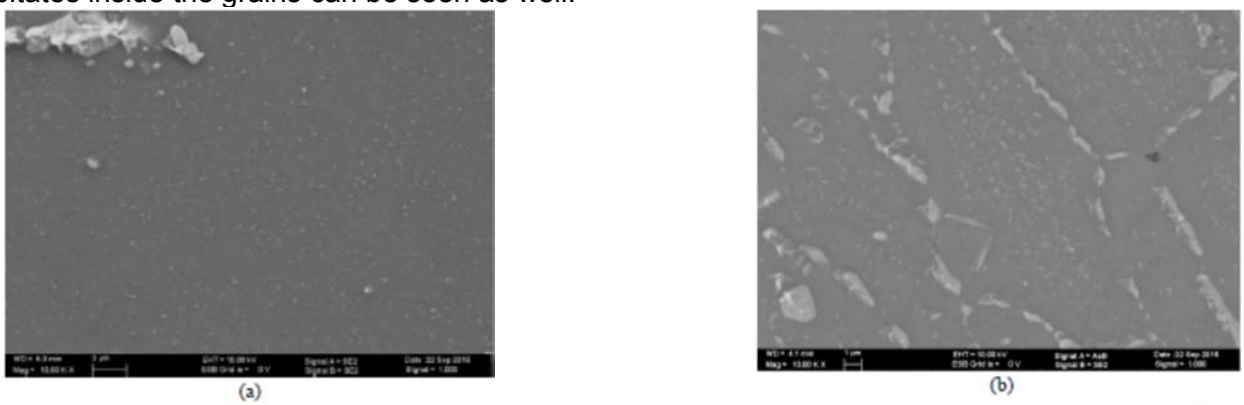

Fig. 11 *HRSEM images of (a) As-recieved material (b) After 170 hour long exposure to 315 ^{0}C*
Sl. 11 *HRTEM slike (a) Primljeni materijal (b) Posle 170 sati dugog izlaganja na 315 ^{0}C*

Systematic precipitation analysis conducted using both TEM and HRSEM indicated that these precipitates can either contain Al, Cu and Mg or can contain just Al and Cu. Examples of such precipitates are given in Fig. 12.

Sistematska analiza taloga sprovedena korišćenjem i TEM i HRSEM pokazala je da ovi talozi mogu da sadrže Al, Cu i Mg ili mogu da sadrže samo Al i Cu. Primeri takvih taloga su dati na slici 12.

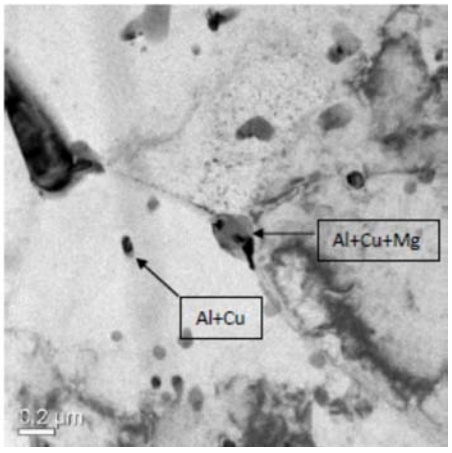

Fig. 12 *BF TEM image of a specimen exposed to 315 ^{0}C for 139 hrs*
Sl. 12 *BF TEM slika uzorka izložena 315 ^{0}C tokom 139 sati*

4. Discussion

As stated earlier clearly shows that the FSW samples exhibited a minimum creep rate that is higher by orders of magnitude than that of the base alloy, tested either under constant or variable load. The stress exponent calculated, namely 4.4, points at dislocation creep, however, the current study brings clear evidence of the microstructure instability during creep. TEM study yielded that high dislocation density and networks were observed at the parent metal (see Fig. 8) while dislocation free grains at the welded nugget (see Fig. 10) point at DRX occurring due to heavy plastic deformation during FSW as stated by Genevois et al. [2 l] and other researchers [17,19]. This conclusion is in line with optical microscopy results. The appearance of submicron dislocation free grains during creep (see Fig. 9) may point also at DRX processes occurring during creep. The material contains in its as received condition coarse precipitates together with evenly dispersed nano-sized ones as can be seen in Fig. 12a, keeping in mind that the thermal condition of the alloy is T3, namely, solution heat treated, cold worked, and naturally aged, the primary coarse precipitates can be due to insufficient solution treatment. Secondary precipitation processes occur then during exposure to creep temperature, this secondary precipitation results in grain boundary decoration, appearance of secondary rod-shaped precipitates and some degree of coarsening of the nano sized precipitates inside the grains. Aging experiments and chemical analysis of the precipitates showed that the secondary precipitates are of both types Al-Cu-Mg and Al-Cu, it can be concluded, therefore, that both S and aging sequences took place. As for the friction stir welded specimens, the situation is even more complicated in that case because the material which has already recrystallized during welding

4. Diskusija

Kao što je ranije navedeno, jasno je vidljivo da su uzorci FSW pokazali minimalnu brzinu puzanja koja je veća za red veličine od one u osnovnom materijalu, testirano ili pod konstantnim ili promenljivim opterećenjem. Izračunati eksponent napona, tačke.4,4 pri puzanju dislokacije, međutim, trenutna studija donosi jasne dokaze o nestabilnosti mikrostrukture tokom puzanja. TEM studija je pokazala da su na osnovnom materijalu primećene visoke gustine dislokacije i mreže (vidi Sl. 8), dok se zrna bez dislokacije u izbočini zavarenoj spoja (vidi Sl. 10) pri DRX-u nastaju usled teške plastične deformacije tokom FSW-a kako su naveli Genevois I dr. [2 l] i drugi istraživači [17,19]. Ovaj zaključak je u skladu s rezultatima optičke mikroskopije. Pojava zrna bez submikronskih dislokacije tokom puzanja (vidi Sliku 9) može ukazivati i pri DRX na procese koji se javljaju tokom puzanja. Materijal sadrži u svom primljenom stanju grube taloge zajedno sa ravnomerno raspodeljenim nano veličine kao što se vidi na slici 12a, imajući u vidu da je termičko stanje legure T3, naime, obrađen termičkim rastvaranjem,, hladno obrađen, i prirodno staren, primarni grubi talozi mogu biti posledica nedovoljnog tretmana rastvora. Postupci sekundarnog taloženja se javljaju tokom izlaganja temperaturi puzanja, ti sekundarni talozi rezultiraju dekorom na granici zrna, pojavom sekundarnih taloga u obliku štapa i određenim stepenom ogrubljenja taloga nano veličine unutar zrna. Eksperimenti starenja i hemijska analiza taloga, pokazali su da su sekundarni talozi , obe vrste Al-Cu-Mg i Al-Cu, pa se može zaključiti da i S i starenje zauzimaju svoje mesto. Što se tiče zavarenih uzoraka trenjem sa mešanjem, situacija je u tom slučaju još složenija jer se materijal koji je već rekristalizovan tokom zavarivanja podvrgava undergoes DRX

during creep so that ultra- fine grains are being created concurrently, in addition, the secondary precipitation processes mentioned above occur during creep of the welded material as well as in the case of the parent material.

5. Conclusions

• The microstructure of AA2024-T3 was found to be unstable at the temperature range of 250-315^{0}C, secondary precipitation was found to take place, this secondary precipitation is responsible for grain boundary decoration and the appearance

• TEM study yielded that the material undergoes DRX during creep

• The material undergoes DRX during the FSW process

• The friction stir welded material, which has already recrystallized during welding, undergoes DRX during creep so that ultra-fine grains are being created concurrently. Precipitation processes at the friction stir welded material occur as well during the process

• The instability of the micro-structure during creep and exposure to high temperature plays an important role in the analysis of the creep results

• Cracking was found to limit the creep resistance of the friction stir welded AA2024

• Further research work is required in order to eliminate the cracking and improve the creep resistance of the friction stir welded AA2024-T3

Acknowledgements

This research project is partially funded by Ort Braude College of Engineering, Israel. The authors wish to thank Dr. Y. Kaufmann for his assistance with the TEM study and Dr. G. Atiya for the TEM specimen preparation. The assistance of Dr. Alexander Katz- Demyanetz with the HRSEM study is highly appreciated.

References

[1] Nakai M and Eto T 2000 Mater. Sci. Eng. A A285(1-2) 62

[2] Huda Z and Edi P 2013 Mater. Des. 46 552

[3] Dursun T and Sutis C 2014 Mater. Des. 56 862

[4] Lumley R N, Morton A J and Polmear I J 2002 Acta Mater. 50(14) 3597

[5] Lumley R N and Polmear 2004 Scripta Mater. 50(9) 1227

[6] Heimerl G J and Farquhart J F 1959 Compressive and tensile creep of 7075-T6 and 2024-T3 Aluminum alloy sheet NASA Technical Note TN D-160

[7] Kloc L, Cerri E, Spigarelli S, Evangelista E and Langdon T G 1996 Mater. Sci. Eng. A, A216(1-2) 161

[8] Kloc L, Cerri E, Spigarelli S, Evangelista E and Langdon T G 1997 Acta Mater. 45(2) 529

[9] Spigarelli S, Cabibbo M, Evangelista E and Langdon T G 2002 Mater. Sci. Eng. A A328(1-2) 39

[10] Lin Y C, Xia Y -C, Jiang Y -Q and Li L -T 2012 Mater. Sci. Eng. A A556 796

[11] Lin Y C, Xia Y -C, Jiang Y -Q, Zhou H -M and Li L –T 2013 Mater. Sci. Eng. A A565 420

DRX tokom puzanja, tako da se istovremeno stvaraju ultrafina zrna, pored toga, gore navedeni sekundarni procesi taloženja nastaju tokom puzanja zavarenog materijala, kao i kod osnovnog materijala.

5. Zaključci

• Otkriveno je da je mikrostruktura AA2024-T3 nestabilna u temperaturnom opsegu 250-315^{0}C, da su se pojavili sekundarni talozi , a ovi sekundarni talozi su odgovorni za dekor granica zrna i izgled

• TEM proučavanje je pokazalo da se tokom puzanja, materijal podvrgava DRX

• Materijal je podvrgnut DRX tokom FSW procesa

• Materijal zavaren trenjem sa mešanjem koji je već rekristalizovao tokom zavarivanja, podvrgava se DRX tokom puzanja tako da se istovremeno stvaraju i ultrafina zrna. Procesi taloženja na materijalu za zavarivanje trenjem dešavaju se tokom procesa

• Nestabilnost mikro strukture tokom puzanja i izloženost visokoj temperaturi igraju važnu ulogu u analizi rezultata puzanja.

• Nađene su prsline koje ograničavaju otpornost na puzanje AA2024 zavarenog trenjem

• Potrebni su dodatni istraživački radovi kako bi se uklonile prsline i poboljšala otpornost na puzanje AA2024 zavarienog trenjem

Zahvalnost

Ovaj istraživački projekat delimično finansira Inženjerski fakultet Ort Braude, Izrael. Autori se zahvaljuju dr. I. Kaufmannu na pomoći u istraživanju TEM-a i dr. G. Atiia na pripremi uzorka TEM-a. Aleksander Katz-Demianetz je pomagao u istraživanju HRSEM-a

[12] Lin Y C, Xia Y -C, Ma X -S, Jiang Y -Q and Chen M –S 2012 Mater. Sci. Eng. A A550 125

[13] Maximov J T, Duncheva G V, Anchev A P and Ichkova M D 2014 Comput. Mater. Sci. 83 391

[14] Wang S C and Starink M J 2005 Int. Mater. Rev. 50(4) 193

[15] Zhang F, Levine L E, Allen A J, Campbell C E, Creuziger A A, Kazantseva N and Ilavsky J 2016 Acta Mater. 111 385

[16] Leal R M and Loureiro A 2006 Mater. Sci. Forum 514- 516 679

[17] Fu R -D, Zhang J -F, Li Y -J, Kang J, Liu H -J and Zhang F -C 2013 Mater. Sci. Eng. A A559 319

[18] Chen Y, Ding H, Li J -Z, Zhao J -W, Fu M -J and Li X –H 2015 Trans. Nonferrous Met. Soc. China 25 2524

[19] Dixit V, Mishra R S, Lederich R J and Talwar R Sci. 2009 Technol. Weld. Join. 14(4) 646

[20] Jones M J, Heurtier P, Desrayaud C, Montheillet F, Allehaux D and Driver J H 2005 Scripta Mater., 52, 693

[21] Genevois C, Deschamps A, Denquin A and Doisneaucottignies B 2005 Acta Mater. 53, 2447

Jacob Kleimana, Yuri Kudryavtsevb

NON-DESTRUCTIVE MEASUREMENTS OF RESIDUAL STRESSES IN STRUCTURAL DETAILS OF BRIDGES
MERENJE ZAOSTALIH NAPONA BEZ RAZARANJA U KONSTRUKCIONIM DELOVIMA MOSTOVA

Originalni naučni rad / Original scientific paper
Rad je u izvornom obliku objavljen u okviru 72. IIW godišnje Skupštine i međunarodne konferencije održane u Bratislavi-Slovačka 07-12. Jula 2019
Rad primljen / Paper received:
Maj 2020.

Adresa autora / Author's address:
Structural Integrity Technologies Inc. (Sintec), Markham, Canada
ajkleiman@sintec.ca, bykudryavtsev@sintec.ca

Ključne reči: nerazorno merenje zaostalih napona, ultrazvučno ispitivanje zaostalih napona, UltraMARS, zaostali naponi u mostovima.

Keywords: non-destructive measurement of residual stresses, ultrasonic testing of residual stresses, UltraMARS, residual stresses in bridges.

Abstract
Bridges are vital in our society for uninterrupted transportation of goods and people on roads and railways and timely maintenance and repair of bridges are of outmost importance. The residual stresses have a significant effect on the process of the initiation and propagation of the fatigue cracks in welded elements and are responsible for many bridge failures.Knowledge of residual stresses, their distribution and their nature is, therefore, of paramount importance in all stages of bridge's design, building and maintenance. Among non-destructive methods for residual stress measurements the use of ultrasonic waves is gaining popularity and acceptance. A portable instrument, UltraMARS that is capable of measuring residual stresses in materials either averaged through thickness or in surface and subsurface layers using ultrasonic waves of different frequencies and displaying the results in a form of a continuous curve on the screen of the instrument was developed and used successfully in many investigations [1, 2].
The main principles of operation and used methodology are briefly discussed, with actual measurement examples using the bulk, the surface and the subsurface presented. A new transducer for measurement of surface and subsurface stresses with a variable base between the ultrasonic wave sender and receiver was designed and manufactured recently. By changing the distance between the sender and receiver it is possible to obtain nondestructively information on residual stress distribution through a certain range of thicknesses of the interrogated materials and structures. Results of calibration of the new variable base ultrasonic transducer (VBUT) for a number of selected materials will be presented.

Abstrakt
Mostovi su od vitalnog značaja za naše društvo radi neprekinutog prevoza robe i ljudi na putevima i železnicama, a blagovremeno održavanje i popravke mostova su od najvećeg značaja. Zaosstali naponi imaju značajan uticaj na proces pokretanja i širenja prslina usled zamora u zavarenim elementima i odgovorni su za mnoge lomove mosta. Znanje o zaostalim naponima, njihovoj distribuciji i njihovoj prirodi su, dakle, od najvećeg značaja u svim fazama projektovanja, izgradnje i održavanja mosta. Među metodama bez razaranja za merenje zaostalih napona, upotreba ultrazvučnih talasa dobija sve veću popularnost i prihvatanje. Razvijen je prenosni instrument, UltraMARS koji je sposoban za merenje zaostalih napona u materijalima bilo u preseku kroz debljinu ili površinskim i podpovršinskim slojevima koristeći ultrazvučne talase različite frekvencije i prikazivanje rezultata u obliku kontinuirane krive na ekranu instrumenta i uspešno se koristi u mnogim istraživanjima [1, 2].
Glavni principi rada i korišćena metodologija su ukratko razmotreni, sa stvarnim primerima merenja koristeći zapreminu, površinu i podpovršinu. Nedavno je dizajniran i proizveden novi pretvarač za merenje površinskih i podpovršinskih napona sa promenljivom bazom između ultrazvučnog talasa i prijemnika. Promenom udaljenosti između odašiljača i prijemnika moguće je dobiti , bez razaranja, informacije o raspodeli zaostalog naprezanja kroz određeni raspon debljina ispitivanih materijala i konstrukcija. Biće predstavljeni rezultati kalibracije novog promenljivog baznog ultrazvučnog pretvarača (VBUT) za određeni broj odabranih materijala.
Takođe su prikazani rezultati zaostalih napona merenih u konstrukcionim delovima mosta koji je

The results of residual stresses measured in structural details of a bridge that was damaged as well as in a number of welded bridges before and after application of improvement treatment used to beneficially redistribute the residual stresses are also presented. The obtained data on residuals stress distribution had proven that the non-destructive ultrasonic method for measurement of residual stresses is a practical and useful tool in maintenance and repair of bridges.

1. Introduction

Bridges are vital in our society for uninterrupted transportation of goods and people on roads and railways and timely maintenance and repair of bridges are of outmost importance. Too many examples exist of catastrophic failures of bridges when these important safety procedures are ignored. A growing number of studies has been and are conducted to improve the existing methods and diagnostic tools and to come up with new procedures and methods for inspection, testing, monitoring and condition assessment, of railway bridges [1-6].

Residual stress can significantly affect engineering properties of materials and structural components, notably, fatigue life, distortion, dimensional stability, corrosion resistance etc.. Such effects usually lead to considerable expenditures in repairs and restoration of parts, equipment and structures. For that reason, the knowledge of residual stresses and their analysis are compulsory stages in the design of structural elements and in the estimation of their reliability under real service conditions.

Systematic studies had shown that welding residual stresses may lead to a drastic reduction in fatigue strength of welded elements. In multi-cycle fatigue (N>106 cycles) the effect of residual stresses can be compared with the effect of stress concentration. Even more significant are the effects of residual stresses on the fatigue life of welded elements in the case of relieving harmful tensile residual stresses and introducing beneficial compressive residual stresses in the weld toe zones. The results of fatigue testing of welded specimens in as-welded condition and after application of ultrasonic peening showed that in case of non-load caring fillet welded joint in high strength steel, the redistribution of residual stresses resulted in approximately two-fold increase in the limit stress range [7, 8].

The residual stresses, therefore, are one of the main factors determining the engineering properties of materials, parts and welded elements and this factor should be taken into account during the design and manufacturing of bridges. Although certain progress has been achieved in the

oštećen kao i u većem broju zavarenih mostova pre i posle primene poboljšanog tretmana korišćenog za korisnu redistribuciju zaostalih napona. Dobijeni podaci o raspodeli zaostalih naprezanja dokazali su da je nerazorna ultrazvučna metoda za merenje zaostalih napona praktično i korisno sredstvo u održavanju i popravci mostova.

1. Uvod

Mostovi su od vitalnog značaja za naše društvo za neprekinuti prevoz robe i ljudi na putevima i železnicama, a blagovremeno održavanje i popravka mostova su od najvećeg značaja. Previše je primera katastrofalnih kvarova mostova kada se ovi važni sigurnosni postupci zanemaruju. Sve veći broj studija je sproveden kako bi se poboljšale postojeće metode i dijagnostički alati i došlo do novih postupaka i metoda za inspekciju, ispitivanje, praćenje i procenu stanja železničkih mostova [1-6].

Zaostali naponi mogu značajno uticati na inženjerska svojstva materijala i konstrukcijskih komponenti, naročito na vek trajanja usled zamora, izobličenje, dimenzionu stabilnost, otpornost na koroziju itd. Takvi efekti obično dovode do znatnih troškova za popravke i restauraciju delova, opreme i konstrukcija. Iz tog razloga, poznavanje zaostalih napona i njihova analiza obavezni su koraci u projektovanju konstrukcijskih elemenata i proceni njihove pouzdanosti u stvarnim uslovima rada.

Sistematske studije su pokazale da zaostali naponi usled zavarivanja mogu dovesti do drastičnog smanjenja čvrstoće zavarenih elemenata. Kod višecikličnog zamora (N> 106 ciklusa) efekat zaostalih napona može se uporediti sa efektom koncentracije napona. Još značajniji su efekti zaostalih napona na vek trajanja usled zamora zavarenih elemenata u slučaju otpuštanja štetnih zateznih zaostalih napona i uvođenja korisnih pritisnih zaostalih napona u zonama podnožja zavarenih spojeva. Rezultati ispitivanja zamorom zavarenih uzoraka u stanju zavarivanja i nakon ultrazvučne obrade površine, pokazali su da u slučaju neopterećenog ugaonog zavarenog spoja od čelika visoke čvrstoće, preraspodela zaostalih napona dovodi do približno dvostrukog povećanja. graničnog opsega napona [7, 8].

Preostali naponi su, dakle, jedan od glavnih faktora koji određuju inženjerska svojstva materijala, delova i zavarenih elemenata i taj faktor treba uzeti u obzir tokom projektovanja i izrade mostova. Iako je postignut određeni napredak u razvoju tehnika za upravljanje zaostalim naponima, još uvek je

development of techniques for residual stress management, a considerable effort is still required to develop efficient and cost-effectiv methods of residual stress measurement and analysis.

2. Measurement of residual stresses by ultrasonic method

The measurements of residual stresses (RS) by UltraMARS® system are based on solid theory, original technique and use of precise instrumentation. It is possible to use ultrasound for measurement of stresses in materials, because, according to the acousto-elastic theory of interaction of ultrasound with materials, the changes in travel velocities (or frequencies) of ultrasound in a material depend linearly on the stresses in the materials over a certain range of stresses [9-11].
For measurement of RS in parts, welded elements and structures, as a prerequisite, the determination of acoustic-elastic coefficients of the considered material has to be performed that is based on measurement of ultrasonic wave velocities in a sample under different loadings and calculation of the acousto-elastic coefficients, based on these measurements. Once the acousto-elastic coefficients are determined, they are added to the UltraMARS® device microprocessor for further computation of RS.

2.1 Residual Stress Measurement System - UltraMARS®

In general, the change in the ultrasonic wave velocity in structural materials under mechanical stress amounts only to tenths of a percentage point. Therefore the equipment for practical application of ultrasonic technique for residual stress measurement should be of high resolution, reliable and fully computerized. The major parts of the developed system for residual stress analysis [12-17] include a measurement unit with supporting software, a preamplifier with a magnetic, electromagnetic or mechanical holder and interchangeable transducers (Fig. 1). For selection of the appropriate reflected wave and tuning in manual mode an oscilloscope is, usually, used. The designed system allows determining uni- and biaxial applied and residual stresses for a wide range of materials and structures.

potreban veliki napor da se razviju efikasne i ekonomične metode merenja i analize zaostalih napona.

2. Merenje zaostalih napona ultrazvučnom metodom

Merenja zaostalih napona (RS) po UltraMARS® sistemu zasnivaju se na teoriji čvrstoće originalnoj tehnici i upotrebi precizne instrumentacije. Moguće je koristiti ultrazvuk za merenje naprezanja u materijalima, jer, prema akustično-elastičnoj teoriji interakcije ultrazvuka sa materijalima, promene brzine kretanja (ili frekvencije) ultrazvuka u materijalu zavise linearno od napona u materijaui u određenom rasponu napona [9-11].
Za merenje RS u delovima, zavarenim elementima i konstrukcijama, kao preduslov, mora se odrediti akustično-elastičnog koeficijent razmatranog materijala koji se zasniva na merenju brzina ultrazvučnih talasa u uzorku pod različitim opterećenjima i izračunavanju akousto-elastičnih koeficijenata na osnovu ovih merenja. Nakon što se utvrde akustično-elastični koeficijenti, oni se dodaju na mikroprocesor uređaja UltraMARS® za dalje računanje RS.

2.1 Sistem za merenje zaostalih napona UltraMARS®

Generalno, promena brzine ultrazvučnog talasa u konstrukcionim materijalima pod mehaničkim naponom iznosi samo desetina procenta. Stoga oprema za praktičnu primenu ultrazvučne tehnike za merenje zaostalih napona treba da bude visoke rezolucije, pouzdana i u potpunosti kompjuterizovana. Glavni delovi razvijenog sistema za analizu zaostalih napona [12-17] uključuju mernu jedinicu sa pratećim softverom, predpojačalo sa magnetnim, elektromagnetnim ili mehaničkim držačem i izmenljive pretvarače (Sl. 1). Za izbor odgovarajućeg refleksnog talasa i podešavanje u ručnom režimu obično se koristi osciloskop. Dizajnirani sistem omogućava određivanje jedno- i dvoosnih i zaostalih napona za širok spektar materijala i konstrukcija.

Fig.1 *Ultrasonic Computerized Complex for residual and applied stress measurement. - Measurement unit with supporting software, (2a) – Preamplifier, (2b) – Magnetic holder, (3) – Transducer, (4) – Oscilloscope, (5) – Sample*
Sl. 1 *Ultrazvučni kompjuterizovani kompleks za merenje zaostalih i primenjenih naprezanja. - Merna jedinica sa pratećim softverom, (2a) - Predpojačalo, (2b) - Magnetni držač, (3) - Pretvarač, (4) - Osciloskop, (5) - Uzorak..*

2.2 Determination of Acousto-elastic Coefficients

The samples for determination of acousto-elastic coefficients can be loaded in compression or in tension. Depending on the loading scheme, the geometry of the sample is selected. Fig. 2a shows a schematic view of a standard sample that is used for determination of acoustoelastic coefficients in tension. Fig. 2b shows a standard sample for determination of acoustoelastic coefficients in compression. During the loading of the sample, the dependence of all three ultrasonic frequencies (the longitudinal and two shear orthogonally polarized) on the applied force should remain linear in the whole range of testing. Fig. 3a and Fig. 3b show laboratory set-ups for measurement of acousto-elastic coefficients using a tension sample or a compression sample, respectively. Fig. 4 presents the linear relationships between all three ultrasonic frequencies and the applied forces obtained in the process of determining the acousto-elastic coefficients.

2.2 Određivanje akustično-elastičnih koeficijenata

Uzorci za određivanje akousto-elastičnih koeficijenata mogu se opteretiti pritiskom ili zatezanjem. U zavisnosti od šeme opterećenja, bira se geometrija uzorka. Sl. 2a prikazuje šematski prikaz standardnog uzorka koji se koristi za određivanje akustično -elastičnih koeficijenata u zatezanju. Sl. 2b prikazuje standardni uzorak za određivanje akousto-elastičnih koeficijenata pri pritisku. Za vreme optrećivanja uzorka, zavisnost sve tri ultrazvučne frekvencije (uzdužna i dva pravougaono polarizovana smicanja) od primenjene sile trebalo bi da ostane linearna u celom opsegu ispitivanja. Sl. 3a i sl. 3b prikazuju laboratorijske postavke za merenje akustično-elastičnih koeficijenata pomoću zateznog uzorka odnosno uzorka pod pritiskom. Sl. 4 prikazuje linearne odnose između sve tri ultrazvučne frekvencije i primenjenih sila dobijenih u procesu određivanja akusto-elastičnih koeficijenata.

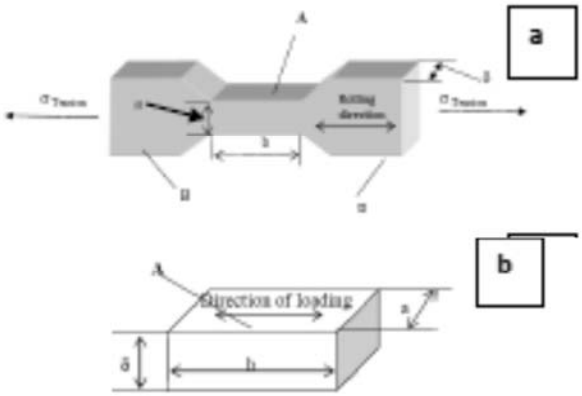

Fig. 2 *Schematic presentation of samples used for determination of the acoustic-elastic coefficients of considered material: a) Tensile sample: a = 50-60 mm; b = 70-80 mm; δ – material thickness; A – zone of installation of ultrasonic gauge(s) during loading of sample; B-grip surfaces; b) Compression sample: a = 50-60 mm; b = 70-80 mm; δ – material thickness; A – surface used for installation of ultrasonic gauge(s).*
Sl. 2 *Šematski prikaz uzoraka koji se koriste za određivanje akusto-elastičnih koeficijenata razmatranog materijala: a) Zatezni uzorak: a = 50-60 mm; b = 70-80 mm? δ - debljina materijala; A - zona postavljanja ultrazvučnih merača tokom optrećenja uzorka; B-stisnuta površina; b) Uzorak pritiskivanja: a = 50-60 mm; b = 70-80 mm; δ - debljina materijala; A - površina koja se koristi za ugradnju ultrazvučnih merača.*

Fig. 3 *General view of the loading set-up for measurement for determination of acousto-elastic constants; a) set-up for measurements on a tension sample; b) set-up for measurements on a compression sample. In both cases the attached to the sample transducer is marked with arrows.*
Sl. 3 *Opšti prikaz podešavanja opterećenja za merenje za određivanje akustično-elastičnih konstanti; a) postavljanje za merenja na uzorku na zatezanje; b) postavljanje za merenja na uzorku na pritisak. U oba slučaja su zakačeni uz uzorke a pretvarači su obeleženi strelicama.*

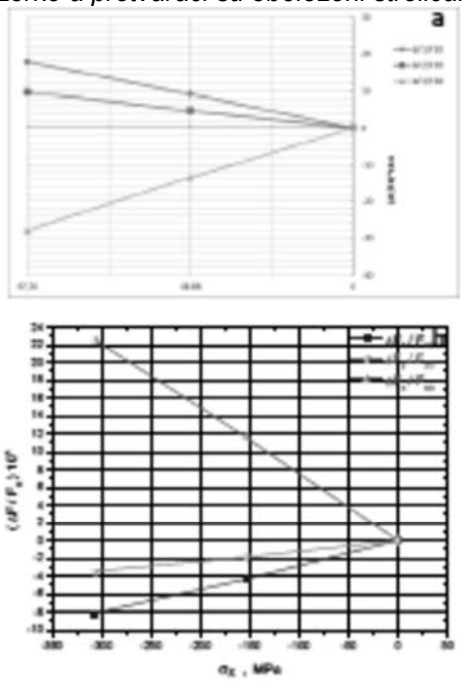

Fig. 4 *Graph of ultrasonic frequencies changes in the sample versus applied stresses; a) applied stresses are tensile; b) applied stresses are compressive.*
Sl. 4 *Grafikon promene ultrazvučnih frekvencija u uzorku u odnosu na primenjena naprezanja; a) primenjeni naponi su zatezni; b) primenjeni naponi su pritisni.*

3. Measurement of residual stresses on bridges

3.1 Evaluation of Residual Stresses in a Damaged Bridge

To evaluate the state of residual stresses in a damaged steel bridge girder region the UltraMARS complex was used. Fig. 5a shows the initial examination of the bridge span that was damaged. Fig. 5b and Fig. 5c show a similar not damaged span of the bridge where residuals stresses were also measured on a girder to compare the state of stresses and assessing the situation..

3. Merenje zaostalih napona na mostovima

3.1 Određivanje zaostalih napona na oštećenom mostu

Za procenu stanja zaostalih napona u području nosača oštećenog čeličnog mosta korišćen je UltraMARS kompleks. Sl. 5a prikazuje početni pregled raspona mosta koji je oštećen. Sl. 5b i Sl. 5c prikazuju sličan neoštećeni deo raspona mosta gde su zaostali naponi mereni i na nosaču da bi se uporedilo stanje napona i procenila situacija..

Fig. 5 *Views of the steel bridge that was struck by a track where the UltraMARS system was used for evaluation of the residual stresses.*

Sl. 5 *Prikazi čeličnog mosta koji udarila staza na kome se sistem UltraMARS koristio za procenu zaostalih napona.*

According to the standard measurement protocol that was developed for measurements of RS in real structures using UltraMARS methodology, firstly, a small cube sample, measuring 50x70x20 mm, similar to the one shown in Fig. 2b was cut and used for measurements of ultrasonic frequencies in compression mode. The sample was installed in a press and the acousto-elastic coefficients were determined using developed methodology (Fig. 4b). The frequencies were measured at three different stresses, i.e at zero stress and at two compressive stresses that were selected at 0.3 σy and 0.6 σy (ultimate tensile strength of the selected material, σy = 385 MPa) and applied to the cube sample.

Fig. 4b presents the frequency changes measured for the longitudinal wave, F1 and two shear orthogonally polarized waves, F2 and F3 as a function of applied load. Three measurements were made, one at no load and at two compressive loads of -116 MPa(0.3 σy) and - 232 MPa (0.6 σy).

Once the acousto-elastic coefficients were established, the actual measurements of residuals stresses in the damaged span and in a span away from the damage were conducted.Fig. 6 presents the region on the bridge that was affected by the impact. The multiple paint layers were removed in the measurement area to ensure that the ultrasound signal is not attenuated.

Prema standardnom protokolu merenja koji je razvijen za merenja RS u stvarnim konstrukcijama po UltraMARS metodologiji, prvo je isečen mali uzorak kocke dimenzija 50x70x20 mm, sličan onome prikazanom na slici 2b i korišćen za merenje ultrazvučnih frekvencija u režimu pritiska. Uzorak je ugrađen u presu i određivani su akustično-elastični koeficijenti primenom razvijene metodologije (slika 4b). Frekvencije su merene na tri različita naprezanja, tj. na nultom naprezanju i na dva pritisna naprezanja koja su odabrana pri 0,3 σy i 0,6 σy (krajnja zatezna čvrstoća izabranog materijala, σi = 385 MPa) i primenjena na uzorak kocke.

Sl. 4b prikazuje promene frekvencije izmerene za uzdužni talas, F1 i dva pravougaona polarizovana talasa smicanja, F2 i F3, kao funkciju primenjenog opterećenja. Obavljena su tri merenja, jedno bez opterećenja i pri dva pritisna opterećenja od -116 MPa (0,3 σy) i - 232 MPa (0,6 σy).

Jednom kada su utvrđeni akustično-elastični koeficijenti, izvršena su stvarna merenja zaostalih napona u oštećenom rasponu i u rasponu udaljenom od oštećenja. Slika 6 prikazuje region na mostu na koji je uticao udar. U području merenja uklonjeno je više slojeva boje da bi se osiguralo da signal ultrazvuka nije oslabljen.

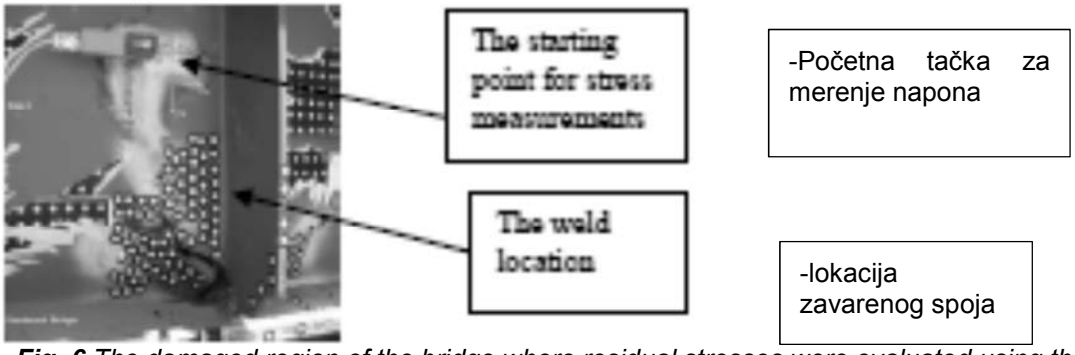

Fig. 6 *The damaged region of the bridge where residual stresses were evaluated using the UltrMARS system.*

Sl. 6 *Oštećena oblast mosta gde su zaostali naponi ocenjeni pomoću UltrMARS sistema*

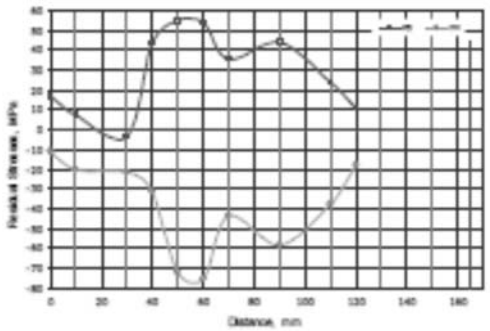

Fig. 7 *Distribution of residual stresses as measured along line #2 (marked in Fig. 6) in the impact zone.*
Sl. 7 *Distribucija zaostalih napona izmerena duž linije 2 (označena na slici 6) u zoni udara.*

One of the results of measurement of the RS in the impact zone is shown in Fig. 7. The distance in Fig. 7 is measured from the starting point, marked in Fig. 6 towards the weld that is marked also in Fig. 6. The two measured components of the residual stress represent the stresses that are perpendicular to the weld (σy) and parallel to the weld (σx).
Fig. 8 presents one of the results of measurement of the RS in a zone selected away from the impact zone (marked with an arrow in Fig. 5b).

Jedan od rezultata merenja RS u udarnoj zoni prikazan je na slici 7. Udaljenost na slici 7 meri se od početne tačke, koja je na slici 6 označena prema zavarenom spoju koji je takođe označen na slici 6. Dve izmerene komponente zaostalog napona predstavljaju napon koji je upravan na zavareni spoj (σy) i paralelan sa zavarom (σx).
Slika 8 prikazuje jedan od rezultata merenja RS u zoni koja je odabrana iz zone udara (obeležena strelicom na slici 5b).

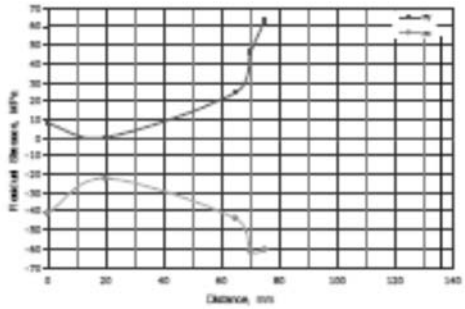

Fig. 8 *Distribution of residual stresses σy and σx measured in a similar girder area on a span of the bridge fare away from the impact zone (as shown in Fig. 5b and Fig. 5c).*
Sl. 8 *Raspodela zaostalih napona σy i σx izmerena u sličnom području nosača na rasponu mosta udaljenom od zone udara (kao što je prikazano na slikama 5b i slici 5c).*

As can be seen from Fig. 7 and Fig. 8, the values and sign of both components of the residual stresses in both measured regions were comparable, suggesting that the impact did not introduce any dangerous stress levels into the structure.

3.2 Measurement of Residual Stresses in a Bridge

Before and After Stress Reliving Operation In a different project, using a similar to the described above approach, average through thickness residual stresses were measured in the main wall of a bridge span near the ends of two welded vertical attachments (Fig. 9) that often are the zones of origination and propagation of fatigue cracks in welded bridges [15].

Kao što se može videti sa slika 7 i slike 8, vrednosti i znak obe komponente zaostalih napona u obe merene oblasti su uporedivi, što sugeriše da udar nije uneo opasne nivoe napona u konstrukciju.

3.2 Merenje zaostlih napona na mostu

Pre i posle operacije oslobađanja od napona u drugom projektu, koristeći sličan gore opisanom pristup, izmereni su po debljini zaostali naponi u glavnom zidu raspona mosta blizu krajeva dva zavarena vertikalna pričvršćenja (slika 9) koji su često zone nastanka i širenja prslina usled zamora u zavarenim mostovima [15].

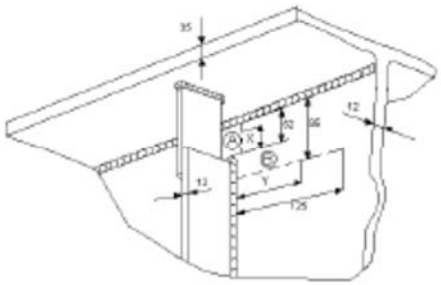

Fig. 9 *Fragment of the railway welded bridge span where the residuals tresses were measured. Zones marked with letters A and B were measured.*
Sl. 9. *Deo raspona železničkog zavarenog mosta na kome su mereni zaostali naponi. Izmerene su zone označene slovima A i B.*

The residual stresses were measured in the same region before and after application of improvement treatment, directed at the beneficial redistribution of the residual stresses. Fig. 10 presents the results of these measurements.

Zaostali naponi mereni su u istoj oblasti pre i posle primene tretmana, usmerenog na korisnu preraspodelu zaostalih napona. Sl. 10 prikazuje rezultate ovih merenja.

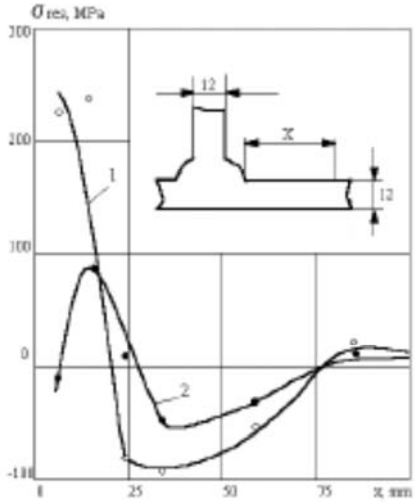

Fig. 10 *Distribution of residual stresses near the fillet weld in the railway bridge span: 1 and 2 – before and after application of the improvement treatment.*
Sl. 10. *Raspodela zaostalih napona blizu zavarenog spoja u rasponu železničkog mosta: 1 i 2 - pre i posle primene tretmana.*

As can be seen from Fig. 10, high tensile residual stresses, reaching 240 MPa were found near the welds before application of improvement treatment. Such high tensile residual stresses are one of the main factors leading to the origination and propagation of the fatigue cracks in welded elements. The application of the improvement treatment caused a dramatic redistribution of the residual stresses near weld zone from initial level of 240 MPA in tension to -10 MPa in compression.

It should be mentioned that the ultrasonic peening as a post-weld treatment process for redistribution and reduction/removal of harmful residual stresses and introduction of beneficial compressive stresses had proven itself as a very useful technique that is applied successfully in rehabilitation and maintenance of bridges [18-21].

Kao što se vidi sa slike 10, pronađeni su visoki zatezni zaostali naponi, dostižući 240 MPa u blizini zavarenih spojeva pre primene tretmana. Tako visoki zatezni zaostali naponi jedan su od glavnih faktora koji vode do nastanka i širenja prslina usled zamora u zavarenim elementima. Primena tretmana uzrokovala je dramatičnu preraspodelu zaostalih napona u blizini zone zavarivanja od početnog nivoa napona od 240 MPA do pritisnog do -10 MPa.

Treba napomenuti da se ultrazvučno „čekičanje“ kao postupak obrade nakon zavarivanja preraspodelom i smanjenjem / uklanjanjem štetnih zaostalih naprezanja i uvođenjem korisnih pritisnih naprezanja pokazao kao vrlo korisna tehnika koja se uspešno primjenjuje u rehabilitaciji i održavanju mostova [18-21

4. Summary

In summary, it was demonstrated that residual stresses can be measured effectively in welded bridge structures using the non-destructive ultrasonic method and, based on it, UltraMARS methodology and equipment. Average through thickness residual stresses were measured in a damaged span of a bridge and away from the damage, and it was shown that the residual stresses in the damaged region did not differ significantly from the control undamaged areas. Also, a dramatic decrease in the residual stresses was measured in a bridge after a post-weld ultrasonic peening treatment, with the stresses near the weld changing from high tensile to compressive.

The substantial technological progress made in the nondestructive measurement of applied and residual stresses by ultrasonic method allowed to use the UltraMARS system that incorporates new software and new functional capabilities, in projects on evaluation of stresses in large welded structures imitating bridge details and in field conditions in bridges. We continue to develop the measurement methodologies and the hardware. Thus, recently, a new methodology and instrumentation, including transducers and other hardware and software for measurement of residual stresses at different depth of material were developed and are being evaluated.

4. Pregled

Ukratko, pokazano je da se zaostali naponi mogu efikasno meriti u zavarenim konstrukcijama mostova upotrebom nerazorne ultrazvučne metode i na osnovu nje, UltraMARS metodologije i opreme. Prosečni zaostali naponi po debljini izmereni su u oštećenom rasponu mosta i dalje od oštećenja, a pokazalo se da se zaostali naponi u oštećenom području ne razlikuju značajno od kontrolnih neoštećenih područja. Takođe, drastično smanjenje zaostalih naprezanja izmereno je na mostu posle tretmana nakon zavarivanja ultrazvučnim „čekičanjem“, pri čemu se naprezanja u blizini zavarenog spoja menjaju iz visokog zateznih u pritisna.

Značajan tehnološki napredak postignut u nerazornom merenju primenjenih i zaostalih napona ultrazvučnom metodom, omogućava upotrebu sistema UltraMARS koji uključuje novi softver i nove funkcionalne mogućnosti, u projektima procene naprezanja u velikim zavarenim konstrukcijama koje imitiraju delove mosta i u poljskim uslovima. Nastavljamo sa razvojem metodologija merenja i hardverom. Tako je nedavno razvijena i vrednovana nova metodologija i instrumentacija, uključujući pretvarače i drugi hardver i softver za merenje zaostalih napona na različitim dubinama materijala.

References

Reference

[1] Integrated Research Project “Sustainable Bridges – Assessment for Future Traffic Demands and Longer Lives” funded by the European Commission within 6th Framework Programme, “Condition assessment and inspection of steel railway bridges, including stress measurements in riveted, bolted and welded structures, Sustainable Bridges SB-3.4 2007-11-30 2 (94), Rev. 2007-11-30.

[2] Lukić, M., Urushadze, S., Fryba, L., et al, 2013, Bridge Fatigue Guidance — Meeting Sustainable Design and Assessment (BRiFaG), Final report, Directorate-General for 00033, 1 July 2008 to 30 June 2011, EUR 25866 EN

[3] Nagy, W., van Bogaert, Ph. And de Backer, H., 2015, Determining Residual Stresses in Welded Connections of Orthotropic Steel Bridge Decks with a Hole-drilling Technique, in “Implementing Innovative Ideas in Structural Engineering and Project Management”, Ed. Saha, S., Zhang, Y., Yazdani, S., and Singh, A., PP. 155-160.

[4] Miyashita, T., Inaba, N., Hirayama, S., Liu, C. and Nagai, M., 2015, Measurement Method for Welding Residual Stress in Steel I-shaped Girder with Thick Flange and its Influence on Load-carrying Capacity for Bending, Journal of JSCE, Vol. 3, 191-208.

[5] Acevedo, C., Evans, A., and Nussbaumer, A., 2012, Neutron diffraction investigations on residual stresses contributing to the fatigue crack growth in ferritic steel tubular bridges, International Journal of Pressure Vessels and Piping , International Journal of Pressure Vessels and Piping 95:31-38.

[6] Clark, Al V., Lozev, M. G. and Fuchs, P.A.,1996, "Bridgesafety evaluation using ultrasonic stress measurement", Proc. SPIE 2946, Nondestructive Evaluation of Bridges and Highways, 13 November 1996); doi: 10.1117/12.259153; https://doi.org/10.1117/12.259153

[7] Trufyakov, V., Mikheev, P. and Kudryavtsev, Y., 1995, “Fatigue Strength of Welded Structures. Residual Stresses and Improvement Treatments”, London. Harwood Academic Publishers GmbH.

[8] Kudryavtsev, Y., 1994, “Effect of Residual Stresses on the Endurance of Welded Joints”, “International Institute of Welding”, IIW Doc. XIII - 1568 - 94.
[9] Hughes, D.S.; Blankenship, E.B.; Mims, R.L. Variation of elastic moduli and wave velocity with pressure and temperature in plastics. J. Appl. Phys. 1950, 21, 294–297. [CrossRef]
[10] Crecraft, D.I. The measurement of applied and residual stresses in metals using ultrasonic waves, J. Sound. Vibr. 1967, 5, 173–192.
[11] Guz’, A.N.; Makhort, F.G., 2000, The Physical Fundamentals of the Ultrasonic Nondestructive Stress Analysis of Solids, Int. Appl. Mech. 2000, 36, PP. 1119–1149.
[12] Kleiman, J. and Kudryavtsev, Y., 2012, “ Residual Stress Management in Welding: Residual Stress Measurement and Improvement Treatments”, in Proceedings of ASME 2012, 31st International Conference on Ocean, Offshore and Arctic Engineering, v 6: Materials Technology; Polar and Arctic Sciences and Technology; Petroleum Technology Symposium, Rio de Janeiro, Brazil, July 1–6, 2012, pp. 73-79.
[13] Kleiman, J. and Kudryavtsev, Y., , 2014, Ultrasonic Measurement of Residual Stresses in Welded Elements, 5TH Annual CWA CanWeld Conference and IIW Congress, Westin Bayshore Hotel Vancouver, Canada, September 28 – October 1, 2014.
[14] Kudryavtsev, Y., 1985, Application of the ultrasonic method for residual stress measurement. Development of fracture toughness requirement for weld joints in steel structures for arctic service. VTT-MET. B-89. Espoo. Finland, pp. 62-76.
[15] Kudryavtsev, Y., Kleiman. J., and Gushcha, O., 2000, Residual Stress Measurement in Welded Elements by Ultrasonic Method, IX International Congress on Experimental Mechanics, Orlando, Florida, USA, June 5-8, 2000, pp. 954-957.
16] Kudryavtsev, Y., Kleiman,. J. and Gushcha, O., 2000, Ultrasonic Measurement of Residual Stresses in Welded Railway Bridge, Structural Materials Technology: An NDT Conference. Atlantic City, NJ. February 28-March 3, 2000, pp. 213-218.
[17] Kudryavtsev, Y., Kleiman, J., Gushcha, O., Smilenko, V., and Brodovy, V., 2004, Ultrasonic Technique and Device for Residual Stress Measurement, X International Congress and Exposition on Experimental and Applied Mechanics, Costa Mesa, California USA, June 7-10, 2004, pp. 1-7.
[18] Ghahremani, K., Walbridge, S., Fatigue Testing and Analysis of Peened Highway Bridge Welds Under In-service Variable Amplitude Loading Conditions, International Journal of Fatigue 33 (2011) 300–312
[19] Hui, J. F., Lloyd, J. B., & Connor, R. J. (2018). Fatigue life improvement of welded girders with ultrasonic impact treatment. West Lafayette, IN: Purdue University. https://doi.org/10.5703/1288284316654
[20] Fisher, J.W. , Statnikov, E. and Tehini, L. Fatigue Strength Improvement of Bridge Girders by Ultrasonic Impact Treatment (UIT), Welding in the World, September 2002, Volume 46, Issue 9–10, pp 34–40.
[21] Günther, H-P, Kuhlmann, U., Dürr, A., Rehabilitation of Welded Joints by Ultrasonic Impact Treatment (UIT), IABSE Symposium, Lisbon, 2005, 1-7.

János Lukácsa, Haidar Mobarkb

Mismatch effect on fatigue crack propagation limit curves of S690QL, S960QL and S960TM type base materials and their gas metal arc welded joints

Uticaj neusklađenosti na granične krive širenja zamornih prslina osnovnih materijala tipa S690KL, S960KL i S960TM i njihovih, elektrolučno u zaštiti gasa, zavarenih spojeva

Originalni naučni rad / Original scientific paper
Rad je u izvornom obliku objavljen u okviru 72. IIW godišnje Skupštine i međunarodne konferencije održane u Bratislavi-Slovačka 07-12. Jula 2019

Rad primljen / Paper received:
Maj 2020.

Adresa autora / Author's address:
Institute of Materials Science and Technology, Faculty of Mechanical Engineering and Informatics, University of Miskolc, Miskolc-
Egyetemvaros, Hungary
ajanos.lukacs@uni-miskolc.hu,
bmobark.mechanical@gmail.com

Ključne reči: Čelici povišene čvrstoće, elektrolučno zavarivanje u zaštiti gasa, efekat neusklađenosti, rast zamornih prslina, dizajna ili granične krive

Keywords: high strength steel, gas metal arc welding, mismatch effect, fatigue crack growth, design or limit curve

Abstract

Nowadays, one of the basic trends in the industry is the environmental impact reduction, in other words the weight decreasing of structural elements and structures, which can be approached by applying different high strength steels. In case of different steel structures, the main manufacturing and joining technology is the welding, the conventional and advanced methods of fusion and pressure welding processes. Beside the weight decreasing, the reliability and safety requirements according to steel structures have significant grown. During the welding process, the welded parts are affected with heat-effect and mechanical loads, which result in inhomogeneous welded joint. The inhomogeneity of the welded joints appears both in microstructural (local) and in geometrical (both local and global) aspects. The changes in microstructure and geometry appear in deflections (basically acceptable), or rather in failures (basically unacceptable); and these influence both the behaviour and the loadability of welded joints. Discontinuities in base materials and their welded joints have especially high danger in case of cyclic loading conditions, which are typical for different structures and structural elements (e.g. bridges, vehicles).

There are different standards and prescriptions containing fatigue crack propagation limit curves and rules for the prediction of the crack growth; simple and two-stage crack growth relationships can be found in the literature, most frequently based on the Paris-Erdogan law. The paper summarizes and presents the results according to our fatigue crack growth investigations on Weldox 700E and Weldox 960E quenched and tempered

Rezime

Danas je jedan od osnovnih trendova u industriji, smanjenje uticaja na životnu sredinu, drugim rečima smanjenje težine konstrukcijskih elemenata i konstrukcija kojima se može pristupiti primenom različitih čelika velike čvrstoće. U slučaju različitih čeličnih konstrukcija, glavna tehnologija proizvodnje i spajanja je zavarivanje, konvencionalnim i naprednim postupcima zavarivanja topljenjem i pritiskom. Pored smanjenja težine, zahtevi za pouzdanost i sigurnost čeličnih konstrukcija su značajno porasli. Tokom procesa zavarivanja, na zavarene delove utiču toplotna i mehanička opterećenja, što rezultira nehomogenim zavarenim spojem. Nehomogenost zavarenih spojeva pojavljuje se i u mikr strukturi (lokalni) i u geometrijskim (i lokalnim i globalnim) aspektima. Promene mikrostrukture i geometrije pojavljuju se u odstupanjima (u osnovi prihvatljivo), ili bolje rečeno u lomovima (u osnovi neprihvatljivo); a oni utiču i na ponašanje i na nosivost zavarenih spojeva. Prekidi u osnovnim materijalima i njihovim zavarenim spojevima imaju posebno veliku opasnost u slučaju cikličnih opterećenja, koji su tipični za različite konstrukcije i konstrukcijske elemente (npr. mostovi, vozila).

Postoje različiti standardi i preporuke koji sadrže granične krive širenja zamorne prsline i pravila za predviđanje rasta prslina; u literaturi se mogu naći jednostavni i dvostepeni odnosi rasta prslina, koji se najčešće zasnivaju na Paris-Erdogan-ovom zakonu. Rad rezimira i prikazuje rezultate prema našim istraživanjima rasta prslina na Weldox 700E i Weldox 960E kaljeni i otpušteni (Q + T) i na Alform 960M termomehanički obrađenom (TM) čeliku

(Q+T) and on Alform 960M thermomechanically treated (TM) high strength steel base materials and their gas metal arc welded joints. The mismatch effect has also been studied; matched, overmatched, undermatched and matched/overmatched (mixed-matched) welded joints were investigated. 15 mm thick plates were used for the investigations, statistical aspects were applied both for presenting the possible crack locations in the real plates, as well as for processing the measured data. Furthermore, the results will be compared with each other, and fatigue crack propagation limit curves will be derived using simple crack growth relationship.

1. Introduction

Reliability of a structural element having crack or cracklike defect under cyclic loading conditions is determined by the geometrical features of the structural element and the flaws, the loading conditions, as well as the material resistance to fatigue crack propagation. There are different documents [1-3], standards and recommendations [4-6] containing fatigue crack propagation limit or design curves and rules for the prediction of the crack growth [6, 7]. The background of the fatigue crack propagation limit curves and the calculations consist of two basic parts: statistical analysis of numerous investigations (fatigue crack propagation tests) and fatigue crack propagation law, frequently the Paris- Erdogan law [8],

$$\frac{da}{dN} = C\Delta K^n, \qquad (1)$$

where da/dN is the fatigue crack growth rate, ΔK is the stress intensity factor range, furthermore C and n are material constants.

The research work and this paper aimed

to characterise the fatigue crack propagation resistance of different high strength structural steels and their welded joints using limit curves [9, 10], based on statistical analysis of test results and the Paris-Erdogan law;

determination of limit curves for different high strength structural steels and their gas metal arc welded joints, under mode I (tension) loading condition.

2. Testing circumstances

2.1 Materials

15 mm thick plates were used for the welding and the base materials and welded joints investigations of SSAB Weldox 700E (abbreviated: W700E) and VOESTALPINE Alform 960M (abbreviated: A960M) material grades. 15 mm thick SSAB Weldox 960E (abbreviated W960E) plate was tested during the

visoke čvrstoće osnovni materijali i njihovi spojevi zavareni elektrolučno u zaštiti gasa. Efekat neusklađenosti je takođe proučen; ispitivani su podudarni, jači (overmatched), slabiji (undermatched), podudarni i podudarni / jači (mešani) zavareni spojevi. Korišćene su ploče debljine 15 mm za istraživanja, primenjeni su statistički aspekti i za predstavljanje mogućih lokacija prslina u stvarnim pločama, kao i za obradu izmerenih podataka. Pored toga, rezultati će se upoređivati jedan sa drugim i sa graničnom krivom širenja zamorne prsline će se izvesti pomoću jednostavnog odnosa rasta prslina.

1. Uvod

Pouzdanost konstrukcijskog elementa koji ima prslinu ili defekt koji liči na prslinu u uslovima cikličnog opterećenja, određuje se pomoću geometrijskih karakteristika konstrukcijskog elementa i nedostaci, uslovi opterećenja, kao i otpornost materijala na širenje prslina. Postoje različiti dokumenti [1-3], standardi i preporuke [4-6] koji sadrže granicu širenja zamorne prsline ili konstrukcijske krive i pravila za predviđanje rasta prsline [6, 7]. Pozadina granične krive širenja zamorne prsline i proračuni se sastoje od dva osnovna dela: statistička analiza brojnih istraživanja (testovi širenja zamorne prsline) i zakon o širenju zamorne prsline, poznat kao Paris- Erdogan-ov zakon [8],

$$\frac{da}{dN} = C\Delta K^n, \qquad (1)$$

gde je da / dN stopa rasta zamorne prsline, ΔK je raspon faktora intenziteta napona, dalje su C i n materijalne konstante materijala .

Istraživački rad i ovaj rad imaju za cilj

- okarakterisati otpornost na širenje prslina kod različitih konstrukcionih čelika visoke čvrstoće i njihovih zavarenih spojeva koristeći granične krive [9, 10], zasnovane na statističkoj analizi rezultata ispitivanja i Paris-Erdogan-ovom zakonu;
- određivanje graničnih krivih za različite konstrukcione čelike visoke čvrstoće i njihove spojeve elektrolučno zavarene u zaštiti gasa, pod režimom opterećenja I (zatezanje)

2. Podaci o ispitivanju

2.1 Materijali

Ploče debljine 15 mm korišćene su za ispitivanje zavarivanja, osnovnih materijala i zavarenih spojeva SSAB Weldox 700E (skraćeno: W700E) i VOESTALPINE Alform 960M (skraćeno: A960M). 15 mm debljina SSAB Weldox 960E (skraćeno

base material examinations, too (designated Weldox 960E-BM and abbreviated W960E); furthermore, 20 mm thick plates were welded and investigated (designated Weldox 960E-WJ and abbreviated W960E). Böhler UNION X85, UNION X90 and UNION X96 (abbreviated X85, X90 and X96, respectively) filler metal were used for the production of welded joits. The chemical composition of the base materials and the filler metals, and the mechanical properties can be seen based on quality certificates in Tab. 1 and Tab. 2, respectively. Based on the data given in Tab. 1 and Tab. 2, it can be found that the two Weldox 960E base materials are the same.

W960E) ploča testirana je i tokom ispitivanja osnovnog materijala (označena Weldox 960E-BM i skraćeno W960E); dalje su zavarene i istražene ploče debljine 20 mm (označene sa Weldox 960E-VJ i skraćeno W960E). Za izradu zavarenih spojeva korišćeni su Bohler UNION X85, UNION X90 i UNION X96 (skraćeno X85, X90 i X96) dodatni materijali. Hemijski sastav osnovnih i dodatnih materijala i mehanička svojstva mogu se videti na osnovu potvrda kvaliteta u Tab. 1 i Tab. 2, respektivno. Na osnovu podataka datih u Tab. 1 i Tab. 2, može se utvrditi da su dva osnovna materijala Weldox 960E ista.

Material Designation	C	Si	Mn	P	S
Weldox 700E	0.14	0.30	1.13	0.007	0.001
Union X85	0.07	0.68	1.62	0.010	0.010
Union X90	0.10	0.8	1.8	N/A	N/A
Weldox 960E-BM	0.16	0.22	1.24	0.009	0.001
Weldox 960E-WJ	0.16	0.23	1.25	0.008	0.001
Alform 960M	0.084	0.329	1.65	0.011	0.0005
Union X96	0.1	0.81	1.94	0.015	0.011
Material Designation	**Cr**	**Ni**	**Mo**	**V**	**Ti**
Weldox 700E	0.30	0.04	0.167	0.011	0.009
Union X85	0.29	1.73	0.61	<0.01	0.08
Union X90	0.35	2.3	0.6	N/A	N/A
Weldox 960E-BM	0.19	0.05	0.581	0.041	0.004
Weldox 960E-WJ	0.20	0.04	0.605	0.04	0.004
Alform 960M	0.61	0.026	0.29	0.078	0.014
Union X96	0.52	2.28	0.53	<0.01	0.06
Material Designation	**Cu**	**Al**	**Nb**	**B**	**N**
Weldox 700E	0.01	0.34	0.001	0.002	0.003
Union X85	0.06	<0.01	N/A	N/A	N/A
Union X90	N/A	N/A	N/A	N/A	N/A
Weldox 960E-BM	0.01	0.056	0.016	0.001	0.003
Weldox 960E-WJ	0.01	0.06	0.016	0.001	0.003
Alform 960M	0.016	0.038	0.035	0.0015	0.006
Union X96	0.06	< 0.01	N/A	N/A	N/A

Tab. 1 *The chemical composition of the examined base materials and filler metals [weight %]*
Tab. 1 *Hemijski sastav ispitivanih osnovnih i dodatnih materijala [težinski %]*

Material Designation	$R_{p0.2}$ [MPa]	R_m [MPa]	A [%]	CVN impact energy [J]
Weldox 700E	791	836	17.0	-40°C: 165
UNION X85	≥ 790	≥ 880	≥ 16.0	-50°C: ≥ 47; 20°C: ≥ 90
UNION X90	≥ 890	≥ 950	≥ 15.0	-50°C: ≥ 47; 20°C: ≥ 90
Weldox 960E-BM	1007	1045	16.0	-40°C: 141
Weldox 960E-WJ	1007	1053	16.0	-40°C: 105
Alform 960M	1051	1058	16.9	-40°C: 40
UNION X96	≥ 930	≥ 980	≥ 14.0	-50°C: ≥ 47; 20°C: ≥ 80

Tab. 2 *The mechanical properties of the examined base materials and filler metals*
Tab. 2 *Mehanička svojstva ispitivanih osnovnih i dodatnih materijala*

2.2 Welding circumstances

The dimensions of the welded workpieces were 300 mm x 125 mm. For the equal stress distribution X-grooved (double V-grooved) welding joints were used, with 80° opening angle and with 2 mm gap between the two plates. The welding equipment was a Daihen Varstroj Welbee Inverter P500L (WB-P500L) MIG/MAG power source; 1.2 mm diameter solid wires and 18% CO2 + 82% Ar gas mixture (M21) were applied. The root layers (2 layers) were made by a qualified welder, while the filler layers (6

2.2 Podaci o zavarivanju

Dimenzije zavarenih komada su bile 300 mm k 125 mm. Za jednaku raspodelu naprezanja korišćeni su X žljebovi (dvostruki V žljebovi), sa uglom otvora 80 ° i zazorom od 2 mm između dve ploče. Oprema za zavarivanje je bio Daihen Varstroj Velbee Inverter P500L (VB-P500L) MIG / MAG izvor napajanja; Primenjene su pune žice prečnika 1,2 mm i gasna smeša 18% CO_2 + 82% Ar (M21). Korenske slojeve (2 sloja) napravio je kvalifikovani zavarivač, dok su slojevi ispune (6 slojeva za ploče debljine 15 mm ili

layers for 15 mm thick plates or 10 layers for 20 mm thick plates) by an automated welding car, in all cases. During the welding process, the workpieces were rotated systematically, after each layer. The applied mismatch characteristics (base materials and filler metals pairing) can be found in Tab. 3.

10 slojeva za ploče debljine 20 mm) izvedeni automatskim zavarivačkim vozilom. Tokom procesa zavarivanja, radni komadi se sistematski rotiraju, nakon svakog sloja. Primenjene karakteristike neusklađenosti (uparivanje osnovnih materijala i dodatnih materijala) mogu se naći u Tab. 3.

Base material	Mismatch type	Filler metal
Weldox 700E	matching (M)	UNION X85
Weldox 700E	overmatching (OM)	UNION X90
Weldox 700E	root layers: matching / filler layers: overmatching (M/OM)	UNION X85/X90
Weldox 960E	matching (M)	UNION X96
Alform 960M	undermatching (UM)	UNION X90
Alform 960M	matching (M)	UNION X96

Tab. 3 *Mismatch characteristics: the applied base materials and filler metals pairing*
Tab. 3 *Karakteristike neusklađenosti: uparivanje osnovnih i dodatnih materijala*

The welding parameters were selected based on both theoretical considerations [11-15] and real industrial applications. A welding monitoring system (WeldQAS, developed and delivered by HKS-Prozesstechnik GmbH [16]) was used for the registration of the welding parameters. Based on the registered data, the applied welding parameters (average or range values) were summarized in Tab. 4. The table shows the welding current (I), the voltage (U) and the welding speed (vw) values, also the preheating (Tpre) and the interpass (Tip) temperatures, with the linear energy (Ev) and the calculated critical cooling time (t8.5/5) values. The parameters of the root and the filler layers were summarized separately

Parametri zavarivanja su odabrani na osnovu teorijskih razmatranja [11-15] i stvarnih industrijskih primena. Za registraciju parametara zavarivanja korišćen je sistem za nadgledanje zavarivanja (WeldQAS, koji je razvio i isporučio HKS-Prozesstechnik GmbH [16]). Na osnovu registrovanih podataka, primenjeni parametri zavarivanja (prosečne ili raspon vrednosti) sumirani su u Tab. 4. U tabeli su prikazane vrednosti struje zavarivanja (I), napona (U) i brzine zavarivanja (vw), takođe temperature predgrevanja (Tpre) i međuslojne temperature (Tip), sa linearnom energijom (Ev) i izračunatom vrednosti kritičnog vremena hlađenja (t8.5 / 5). Parametri za sloja korena i slojeve ispune su sažeti odvojeno.

Base material / filler metal	Layer	T_{pre}, T_{ip} [°C]	I [A]	U [V]
W700E / X85 W700E / X 90 W700E / X85/X90	1-2 root	150	130-140	19.0-20.5
	3-8 filler	180	280-300	28.5-29.5
W960E / X96	1 root	200	96	17.3
	2 root	180	194	22.0
	3-12 filler	150	298-308	29.0-31.0
W960M / X90 W960M / X96	1-2 root	60	130-140	19.0-20.5
	3-8 filler	150	270-300	27.0-28.0
Base material / filler metal	**Layer**	v_w [cm/min]	E_v [J/mm]	$t_{8,5/5}$ [s]
W700E / X85 W700E / X 90 W700E / X85/X90	1-2 root	20	700-750	7-8
	3-8 filler	40	1000-1100	9-11
W960E / X96	1 root	11	727	6.7
	2 root	27	764	6.5
	3-12 filler	45	940-1000	7-8
W960M / X90 W960M / X96	1-2 root	20	700-750	7-8
	3-8 filler	30-45	900-1400	7-15

Tab. 4 *Applied welding parameters*
Tab.4 *Primenjeni parametri zavarivanja*

2.3 Fatigue crack growth tests

The FCG tests were executed on three-point bending (TPB) specimens, nominal W values were 26 mm (t = 15 mm) and 28 mm (t = 20 mm), and 13 mm (t = 15 mm) and 18 mm (t = 20 mm) for the base materials and the welded joints, in the 21 and 23 directions, respectively. The position of the notches correlated with the rolling direction (T-L, L-T, T-S and L-S). The positions of the cut specimens from the and 23W) were used (Fig. 2). Fig. 3 shows one possible location of the noth in the thickness direction (23W). welded joints is shown in Fig. 1, 21 and 23 directions (21W).

2.3 Testovi rasta zamorne prsline

Testovi rasta zamorne prsline (FCG)su izvedeni na uzorcima savijanjem u tri tačke (TPB), nominalne vrednosti W su bile 26 mm (t = 15 mm) i 28 mm (t = 20 mm), a 13 mm (t = 15 mm) i 18 mm (t = 20 mm) za osnovne materijale i zavarene spojeve, u smeru 21 i 23, respektivno. Položaj zareza je u korelaciji sa pravcem valjanja (T-L, L-T, T-S i L-S). Korišćeni su položaji isečenih uzoraka od i 23W) (Sl. 2). Sl. 3 prikazuje jednu moguću lokaciju zareza u pravcu debljine (23W). zavareni spojevi prikazani su na slikama 1, 21 i 23 smera (21W).

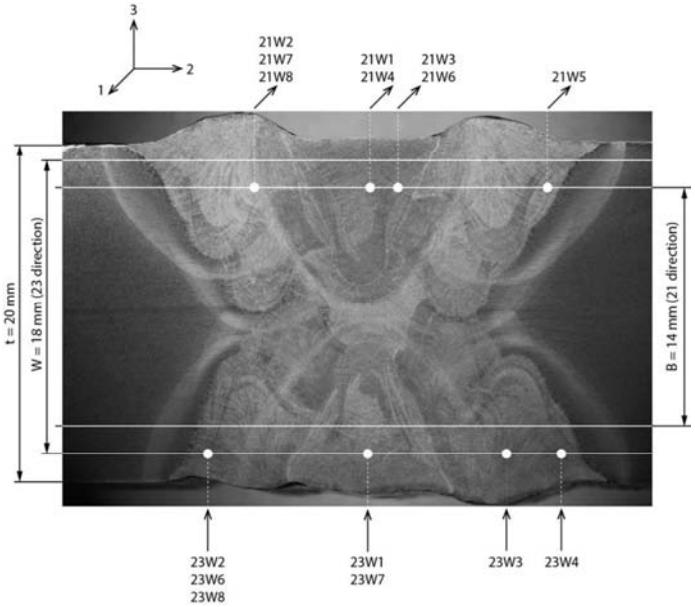

Fig. 1 *TPB specimen locations in the Weldox 960E / UNION X96 welded joints with the crack paths (21W and 23W)*
Sl. 1 *Lokacije uzoraka za savijanje u tri tačke (TPB) Weldox 960E / UNION X96 zavarenim spojevima sa prslinama (21W i 23W)*

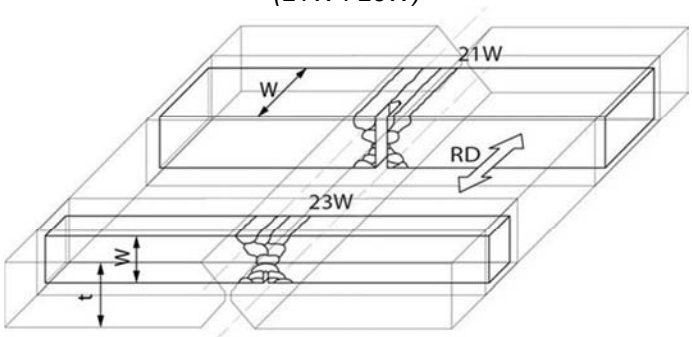

Fig. 2 *TPB specimen locations in the welded joint with the notch directions (RD = rolling directions)*
Sl. 2 *Položaji uzoraka TPB u zavarenom spoju sa smerovima zareza (RD = pravci valjanja)*

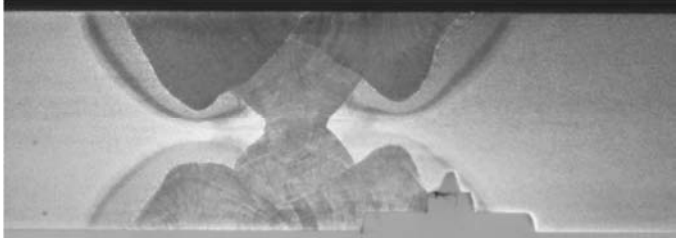

Fig. 3 *One possible location of the notch in the thickness direction*
Sl. 3 *Jedno moguće mesto zareza u smeru debljine*

The notch locations, the notch distances from the centreline of the welded joints, were different, therefore the positions of the notches and the crack paths represent the most important and the most typical crack directions in a real welded joins. Post-weld heat treating was not applied after welding on GMAW joints (investigations in as-welded condition).

The FCG examinations were performed with tensile stress, R = 0.1 stress ratio, sinusoidal loading wave form, at room temperature, and on laboratory air, using MTS type electro-hydraulic testing equipment. The loading frequency was f = 20 Hz for two-thirds of the growing crack's length, approximately, and it was f = 5 Hz for the last third. The propagating crack was registered with optical method, using video camera and hundredfold magnification (N = 100x).

Lokacije zareza, udaljenosti zareza od središnje linije zavarenih spojeva, bili su različiti, pa su položaji zareza i prslina najvažniji i najtipičniji pravci prslina u stvarnim zavarenim spojevima. Termička obrada posle zavarivanja na zavarenim spojevima GMAW-MIG/MAG (ispitivanja u stanju zavarivanja) nije primenjena.

FCG ispitivanja izvedena su sa zateznim naponom, odnosom napona R = 0,1, sinusoidnim talasnim opterećenjem, na sobnoj temperaturi i na laboratorijskom vazduhu, koristeći elektro-hidrauličku opremu za ispitivanje tipa MTS. Frekvencija opterećenja bila je f = 20 Hz za dve trećine rastuće dužine prsline, otprilike, i bila je f = 5 Hz za poslednju trećinu. Propagirajuća prslina registrovana je optičkim metodama, korišćenjem video kamere i uvećanjem od 100 puta (N = 100x).

3. Results of examinations

3.1 Hardness distribution

HV10 hardness values were measured along two lines, as it can be seen in Fig. 4, furthermore Fig. 5 shows the hardness distributions (Weldox 700E / UNIONX85/UNION X90).

3. Rezultati ispitivanja

3.1 Raspodela tvrdoće

Vrednosti tvrdoće HV10 merene su duž dve linije, kao što se može videti na slici 4, a na slici 5 prikazane su distribucije tvrdoće (Weldox 700E / UNIONKS85 / UNION X90).

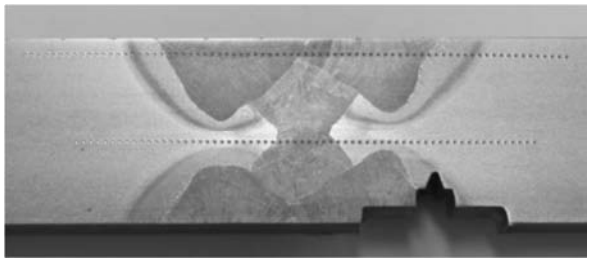

Fig. 4 *Two lines for hardness tests*
Sl. 4 *Dve linije za ispitivanja tvrdoće*

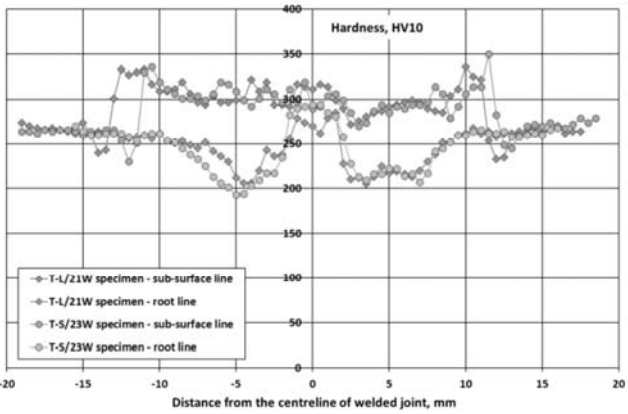

Fig. 5 *Hardness distributions measured on Weldox 700E / UNIONX85/UNION X90 specimen*
Sl. 5 *Raspodela tvrdoće merena na uzorku Weldox 700E / UNIONX85/UNION X90*

3.2 Fatigue crack growth tests

The next figures and Table 5 show selected experimental results on Weldox 700E / UNIONX85/UNION X90 welded joints. The crack length vs. number of cycles curves can be seen in different orientation in Fig. 6 and Fig. 7, and the

3.2 Testovi rasta zamorne prsline

Sledeće slike i tabela 5 prikazuju odabrane eksperimentalne rezultate na Weldox 700E / UNIONKS85 / UNION Ks90 zavarenim spojevima. Dužina prsline naspram krivih broja ciklusa može se videti u različitoj orijentaciji na Sl. 6 i Sl. 7, a

calculated stress intensity factor range vs. fatigue crackgrowth rate values are shown in Fig. 8 (WM = weld metal, HAZ = heat affected zone, BM = base material).

izračunati raspon faktora intenziteta napona u odnosu na vrednosti brzine rasta zamorne prsline,prikazan je na Sl. 8 (WM = metal šava, HAZ = zona pod uticajem toplote, BM = osnovni materijal).

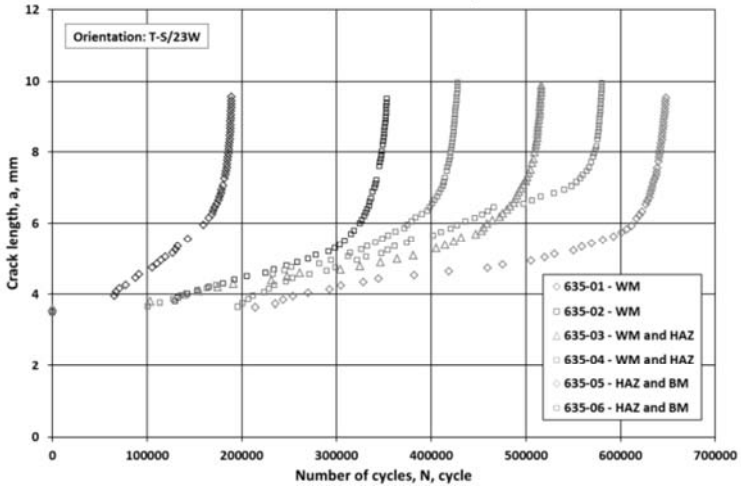

Fig. 6 *Crack length vs. number of cycles curves in T-S/23W orientation (Weldox 700E / UNIONX85/UNION X9*
Sl. 6 *Dužina prsline naspram broja ciklusa na pravcu T-S/23W (Weldox 700E / UNIONX85/UNION X90)0)*

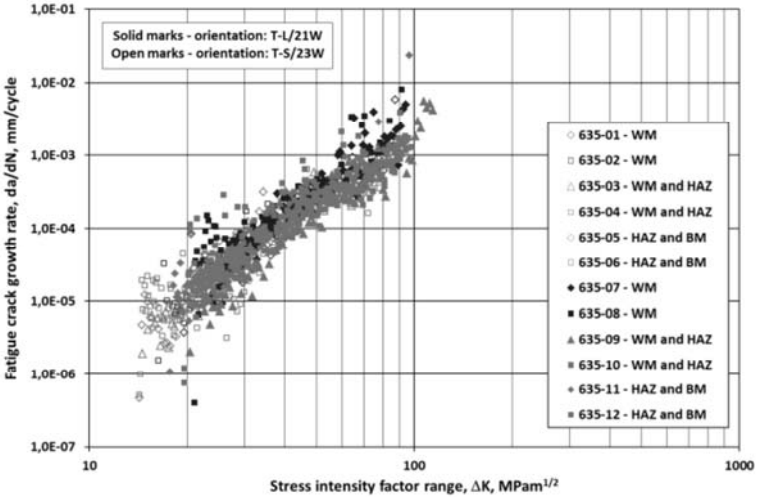

Fig. 8 *Results of FCG tests on Weldox 700E / UNIONX85/UNION X90 welded joints (altogether 12 specimens)*
Sl. 8 *Rezultati FCG testova na zavarenim spojevima Weldox 700E / UNIONKS85 / UNION X90 (ukupno 12 uzoraka)*

Secant method [17] was used to evaluate the fatigue crack growth data. The constants (C and n) of the Paris-Erdogan relationship [8] were calculated using the least squares regression method, and the fatigue fracture toughness (ΔKfc) values were determined using the crack length on the crack front measured by stereo microscope. The data belonging to stage II of the kinetic diagram of fatigue crack propagation have been eliminated during the least square regression analysis, for each specimen, systematically.

Tab. 5 summarizes the FCG test results executed on specimens cut from Weldox 700E / UNIONX85/UNION X90 welded joints (Sp ID = specimen ID, Co coe = correlation coefficient).

Za procenu podataka rasta prslina usled zamora korišćena je metoda sekante [17]. Konstante (C i n) Paris-Erdogan-ovog odnosa [8] izračunate su korišćenjem metode najmanje kvadratne regresije, a vrednosti žilavosti preloma usled zamora (ΔKfc) određene su korišćenjem dužine prsltine na prednjoj strani merene stereo mikroskopom. Podaci koji pripadaju II stadijumu kinetičkog dijagrama širenja prslina usled zamora eliminisani su tokom analize najmanje kvadratne regresije, za svaki uzorak, sistematski.

Tabela. 5 rezimira rezultate FCG ispitivanja izvršenih na uzorcima iz Weldox 700E / UNIONKS85 / UNION X90 zavarenih spojeva (Sp ID = ID uzorak, Co koeficijent korelacije).

Sp ID	Crack path	C [MPam$^{1/2}$, mm/cycle]	n	Co coe [-]	ΔK_{th} [MPam$^{1/2}$]
635-01	WM	5.23E-10	3.30	0.9549	91.3
635-02	WM	8.03E-10	3.21	0.9496	76.2
635-03	WM / HAZ	3.45E-10	3.43	0.9632	80.1
635-04	WM / HAZ	4.62E-10	3.27	0.9205	82.1
635-05	HAZ / BM	2.20E-10	3.61	0.9372	68.1
635-06	HAZ / BM	2.13E-09	2.94	0.9309	82.9
635-07	WM	4.42E-10	3.44	0.9454	95.7
635-08	WM	2.72E-09	2.97	0.9274	96.0
635-09	WM / HAZ	2.88E-10	3.36	0.9599	117.0
635-10	WM / HAZ	5.07E-09	2.76	0.9285	98.8
635-11	HAZ / BM	8.64E-10	3.20	0.9613	102.9
635-12	HAZ / BM	2.23E-09	2.94	0.9354	100.0

Tab. 5 *Fatigue crack propagation test results executed on specimens cut from Weldox 700E / UNIONX85/UNION X90 welded joints*

Tab. 5. *Rezultati ispitivanja širenja prslina na uzorcima od Weldox 700E / UNION X85 / UNION X90 zavarenih spojeva*

4. Determination of fatigue crack propagation limit curves

Kinetic diagrams of fatigue crack growth can be simplified and described using both simple and two-stage crack growth relationships, as it can be seen in Fig. 9, based on [6]. (In BS 7910 m is used as Paris-Erdogan exponent, istead of n.) According to the main aim of our research work and the paper, the simple crack growth relationship was selected and used.

4. Određivanje graničnih kriva širenja prslina zamora

Kinetički dijagrami rasta prslina usled zamora mogu se pojednostaviti i opisati upotrebom jednostavnih i dvostepenih odnosa rasta prslina, kao što se može videti na slici 9, na osnovu [6]. (U BS 7910 m koristi se kao eksponent Paris-Erdogan, umesto n..) Prema glavnom cilju našeg istraživačkog rada i rada odabran je i korišćen jednostavan odnos rasta prslina.

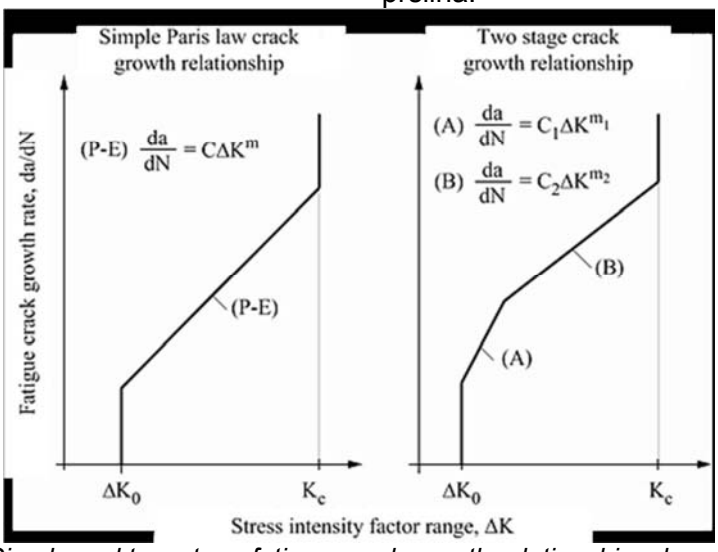

Fig. 9 *Simple and two-stage fatigue crack growth relationships, based on [6]*

Sl. 9 *Jednostavni i dvostepeni rast zamorne prsline, zasnovan na [6]*

Based on the experimental data and results, fatigue crack propagation limit curves can be determined. Generally, the determination of the fatigue design curves consists of six steps, as follows [10]. First step: determination of measuring values, the threshold stress intensity factor range (ΔKth), if available, the two parameters of the Paris-Erdogan law (in our case C and n) and the fatigue fracture toughness (ΔKfc). Second step: classification of measured values into statistical samples, on the basis of calculated test results, applying Wilcoxon matched pairs test. Third step: selection of the distribution function type using Shapiro-Wilk, Kolmogorov- Smirnov and chi square

Na osnovu eksperimentalnih podataka i rezultata mogu se odrediti granične krive širenja prslina usled zamora. Uopšteno, utvrđivanje krivih zamora sastoji se od šest koraka, kako sledi [10]. Prvi korak: određivanje mernih vrednosti, raspon faktora intenziteta praga napona (ΔKth), ako su dostupni, dva parametra Paris-Erdoganovog zakona (u našem slučaju C i n) i žilavost preloma usled zamora (ΔKfc). Drugi korak: klasifikacija izmerenih vrednosti u statističke uzorke, na osnovu izračunatih rezultata ispitivanja, primenom testa Wilcokon-ovih podudarnih parova. Treći korak: izbor vrste funkcije distribucije korišćenjem Shapiro-Wilk, Kolmogorov-Smirnov i kvadrata chi

(χ^2) goodness of fit tests (testing if sample data fits a distribution from a certain population, i.e. a population with a normal or a Weibull distribution), at a level of significance ε= 0.05. After the analysis, it was concluded, that only the three parameter Weibull-distribution function is suitable for describing all the configured samples. Fourth step: calculation of the parameters of the three parameter Weibull-distribution functions. The parameters of the distribution functions were calculated for all the configured samples using the

$$F(x) = 1 - \exp\left[-\left(\frac{x - N_0}{\beta}\right)^{1/\alpha}\right] \quad (2)$$

equation, where N0 is the threshold parameter, α is the shape parameter and β is the scale parameter. Fifth step: selection of the characteristic values of the distribution functions. Considering the influencing effects of the material parameters on the life-time estimation, characteristic values of ΔKth, n and ΔKfc were selected. The threshold stress intensity factor range (ΔKth) is that value which belongs to the 95% probability, the exponent of the Paris-Erdogan law (n) is that value which belongs to the 5% probability and the fatigue fracture toughness (ΔKfc) is that value which belongs to the 5% probability of the relevant Weibull-distribution function. The Paris-Erdogan constant (C) can be calculated on the material group (in our case steels) dependent correlation between C and n. The describen fith step can be seen in Fig. 10, schematically. Sixth step: calculation of the parameters of the limit curves.

The main characteristics of the determined limit curves can be found in Tab. 6 (M t = Mismatch type, Ref = reference). In those cases, when the orientation and/or the path of the propagating crack is known, the values in Tab. 6 can be directly used. In those cases, when n and ΔKfc values calculated in different directions (T-L and L-T vs. T-S, or 21W vs. 23W) are significantly different, and the orientation and/or the growing crack path is not known, the lowest value should be considered from the related ones. The unambiguous determination of the design curves in the near threshold region (near ΔKth) is difficult. On the one hand, if the threshold stress intensity factor range value (ΔKth) is not known, values can be found in the literature (e.g. [21-23]) are usable; furthermore, in special or particular cases, results of virtual testing [24] can be applied, too. On the other hand, the threshold stress intensity factor range value (ΔKth), must be reduced by tensile residual stress field and may be increased by compressive residual stress field (e.g. welding residual stresses).

χ^2 ispravnosti testova (ispitivanje da li uzorak podataka odgovara distribuciji iz određene zastupljenosti, tj. zastupljenosti sa normalnom ili Weibull funkcija distribucije), na nivou značajnosti ε= 0,05. Nakon analize zaključeno je da su samo tri parametra Weibull funkcije distribucijeije pogodne za opisivanje svih konfigurisanih uzoraka. Četvrti korak: izračunavanje parametara tri parametrske funkcije Weibull-distribucije. Parametri distribucijskih funkcija su izračunati za sve konfigurisane uzorke koristeći

$$F(x) = 1 - \exp\left[-\left(\frac{x - N_0}{\beta}\right)^{1/\alpha}\right] \quad (2)$$

jednačinu, gde je N0 parametar praga, σ je parametar oblika, a β je parametar skale. Peti korak: izbor karakterističnih vrednosti distributivnih funkcija. S obzirom na uticaj parametara materijala na procenu životnog veka, odabrane su karakteristične vrednosti ΔKth, n i ΔKfc. Raspon faktora intenziteta graničnog naprezanja (ΔKth) je vrednost koja pripada verovatnoći od 95%, eksponent Paris-Erdogan-ovog zakona (n) je ta vrednost koja pripada verovatnoći od 5%, a žilavost loma zamora (ΔKfc) je ta vrednost koja pripada verovatnoći od 5% za relevantnu funkciju distribucije Weibull-a. Konstanta Paris-Erdogan-a (C) može se izračunati na osnovu grupe materijala (u našem slučaju čelika) zavisne korelacije između C i n. Opisani korak može se šematski videti na slici 10. Šesti korak: izračunavanje parametara granične krive.

Glavne karakteristike utvrđenih graničnih krivih mogu se naći u Tab. 6 (M t = Tip neusklađenosti, Ref = referenca). U onim slučajevima, kada je poznata orijentacija i / ili putanja širenja prslina, vrednosti u Tab. 6 se mogu direktno koristiti. U onim slučajevima, kada su n i ΔKfc vrednosti izračunate u različitim smerovima (TL i LT u odnosu na TS, ili 21W u odnosu na 23W) značajno se razlikuju, a orijentacija i / ili put rastuće prsline nije poznat, najniža vrednost treba da bude uzeta u obzir. Teško je nedvosmisleno odrediti dizajn krive u blizini praga (blizu ΔKth). S jedne strane, ako vrednost raspona faktora intenziteta praga naprezanja (ΔKth) nije poznata, vrednosti se mogu naći u literaturi (npr. [21-23]) koje su upotrebljive; Nadalje, u specijalnim ili posebnim slučajevima, mogu se primeniti i rezultati virtualnog testiranja [24]. S druge strane, vrednost raspona faktora intenziteta napona (ΔKth) mora se smanjiti zateznim zaostalim poljem i može povećati pritisnim poljem zaostalih napona (npr. zaostali naponi usled zavarivanja).

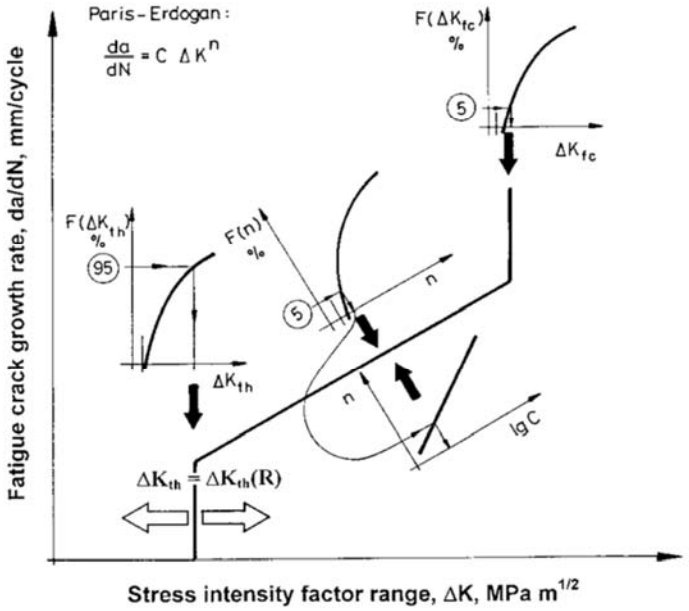

Fig. 10 *The proposed method for determination of fatigue crack propagation limit curves*
Sl. 10 *Predloženi postupak za određivanje graničnih krivih širenja prslina usled zamora*

BM	M t	Orientation	n	C	ΔK_{fc}	Ref
			[MPam$^{1/2}$, mm/cycle]			
W700E	BM	T-L, L-T	1,70	8,09E-07	101	[18]
		T-S	1,50	2,06E-06	75	
W700E	M	T-L/21W	4,10	1,12E-11	105	[18]
		T-S/23W	2,30	4,93E-08	80	
W700E	OM	T-L/21W	1,85	4,02E-07	96	[18]
		T-S/23W	1,90	3,19E-07	61	
W700E	M/OM	T-L/21W	2,67	8,88E-09	90	this
		T-S/23W	2,85	3,87E-09	67	study
W960E	BM	T-S, L-S, T-L	1,80	3,50E-07	94	[19]
W960E	M	T-L/21W, T-S/23W	2,75	1,03E-08	93	[20]
A960M	BM	T-L, L-T	1,82	4,63E-07	116	[18]
		T-S	1,75	6,41E-07	87	
A960M	UM	T-L/21W	2,40	3,10E-08	115	[18]
		T-S/23W	2,15	9,93E-08	67	
A960M	M	T-L/21W	1,90	3,19E-07	114	[18]
		T-S/23W	2,75	6,06E-09	82	

Tab. 6 *Characteristics of the determined fatigue crack propagation limit curves*
Tab. 6. *Karakteristike utvrđenih graničnih krivih širenja prslina usled zamora*

5. Summary and conclusions

Based on our investigations and their results the following conclusions can be drawn.

The results of the executed investigations justified the necessity of statistical approaches, especially referring to the directions of the base materials and the welded joints, and the determination of the number of the tested specimens.

The applied gas metal arc welding process and the used technological parameters are suitable for production welded joints with appropriate quality,

5. Rezime i zaključci

Na osnovu naših istraživanja i njihovih rezultata mogu se doneti sledeći zaključci.

Rezultati izvršenih istraživanja opravdali su neophodnost statističkih pristupa, posebno se odnose na smer osnovnog materijala i zavarene spojeve, kao i određivanje broja ispitivanih uzoraka.

Primenjeni postupak elektrolučnog zavarivanja u zaštiti gasa i korišćeni tehnološki parametri pogodni su za izradu zavarenih spojeva odgovarajućeg kvaliteta, pri čemu odgovarajući kvalitet sadrži

where the appropriate quality contains the eligible resistance to fatigue crack propagation.
The welding causes unfavourable effects both on the mechanical properties and the fatigue crack growth resistance of the high strength steels.
The average values of the Paris-Erdogan exponents (n) of Weldox 700E and Alform 960M base materials in the T-L and L-T directions and of the Weldox 960Q base material in the T-S and L-S directions are significantly not different, which means equal fatigue crack growth resistance in these orientations. The average values of the Paris-Erdogan exponent (n) of Weldox 700E and Alform 960M base materials in the T-S orientation and of the Weldox 960Q base material in the T-L orientation are significantly different. The fatigue crack growth resistance of the Weldox 700E material is more unfavourable in T-S direction. The material strength category (in our case 690 MPa or 960 MPa) and the production condition (in our case quenching and tempering or thermomechanically treating) cause significant effect on the fatigue crack growth resistance, too.
The average values of the Paris-Erdogan exponents (n) of the matching (M), overmatching (OM), matching / overmatching (M/OM) and undermatching (UM) conditions of the investigated welded joints were statistically higher than the exponents of the concerning base materials.
The average value of the Paris-Erdogan exponent (n) of the overmatching (OM) welded joint of the Weldox 700E is lower than the exponent of both the matching (M) and the matching/overmatching (M/OM) conditions. The fatigue crack growth resistance under overmatching (OM) condition is lower than both matching (M) and matching/overmatching (M/OM) conditions. It means that the matching/overmatching (M/OM) mismatch type is more beneficial than the overmatching (OM) type.
The average value of the Paris-Erdogan exponent (n) of the matching (M) welded joint of the Alform 960M is lower than the exponent of the undermatching (UM) condition. The fatigue crack growth resistance under matching (M) condition is lower than undermatching (UM) condition.
The determined results fundamentally refer to reliable and reproducible examinations. Unfortunately, the standard deviation coefficients are in some cases too high (Paris- Erdogan exponent (n), T-S, 21W and 23W orientations).
Based on these results and the used methods fatigue crack propagation limit curves can be determined for the investigated high strength base materials and their gas metal arc welded joints,

prihvatljivi otpor protiv širenja prslina.
Zavarivanje izaziva nepovoljne efekte i na mehanička svojstva i na otpornost na rast prslina kod čelika visoke čvrstoće.
Prosečne vrednosti Paris-Erdogan-ovih eksponenata (n) Weldox 700E i Alform 960M osnovnih materijala u pravcima TL i LT i materijala Weldox 960K u pravcu TS i LS značajno se ne razlikuju, što znači jednak otpor rastu prslina usled zamora u ovim orijentacijama. Prosečne vrednosti Paris-Erdogan-ovih eksponenata (n) Weldox 700E i Alform 960M osnovnih materijala u T-S orijentaciji i Weldox 960K osnovnog materijala u T-L orijentaciji su značajno različite. Otpor na rast prslina usled zamora materijala Weldox 700E je nepovoljniji u T-S smeru. Kategorija čvrstoće materijala (u našem slučaju 690 MPa ili 960 MPa) i stanje proizvodnje (u našem slučaju kaljenje i otpuštanje ili termomehanička obrada) takođe imaju značajan uticaj na otpornost na rast prslina.
Prosečne vrednosti Paris-Erdogan-ovih eksponenata (n) kod uslova podudaranja (M), jačeg (OM), podudaranja / jačeg (M / OM) i slabijeg (UM) ispitivanih zavarenih spojeva su statistički veće od eksponenata za osnovne materijale.
Prosečna vrednost Paris-Erdogan eksponenta (n) jačeg (OM) zavarenog spoja Weldox 700E je niža od eksponenta i uslova podudaranja (M) i podudaranja / jačeg (M / OM) uslova. Otpor rasta prslina usled zamora pod uslovima jačeg (OM) je niži od uslova podudaranja (M) i uslova podudaranja / jaćeg (M / OM). To znači da je tip neusklađenosti, podudaranje / jači (M / OM), povoljniji od tipa jačeg (OM).
Prosečna vrednost Paris-Erdogan eksponente (n) podudarajućeg (M) zavarenog spoja Alform 960M je niža od eksponenta za uslov slabijeg (UM). Otpor na rast prslina usled zamora pod podudarajužim (M) uslovima je niži od uslova slabijeg (UM).
Utvrđeni rezultati se u osnovi odnose na pouzdana i ponovljiva ispitivanja. Nažalost, standardni koeficijenti devijacije su u nekim slučajevima previsoki (Paris-Erdogan eksponent (n), T-S, 21W i 23W orijentacije).
Na osnovu ovih rezultata i korišćenim metodama mogu se utvrditi granične krive širenja prslina za ispitivane osnovne materijale i njihove zavarene spojeve postupkom elektročućnog zavarivanja u zaštiti gasa, upotrebom pojednostavljene metode [6]. Granične krive s jedne strane tačno odražavaju karakteristike rasta prslina usled zamora i osnovnih materijala i zavarenih spojeva, s druge strane se mogu koristiti za kritičku procenu inženjerskih analiza (ECA) i proračune strukturnog integriteta:

using simplified method [6]. The limit curves on the one hand correctly reflect the fatigue crack growth characteristics of both the base materials and the welded joints, on the other hand are usable for engineering critical assessment (ECA) and structural integrity calculations:
- determination of propagable an critical crack sizes;
- calculation of lifetime determined by the propagable crack size;
- calculations of remaining lifetime functions, influences on the lifetime values and lifetime function (in other words parameter study);
- reliability of remaining lifetime estimation;
- calculation of damage parameter and damage function [25].
Further examinations required in order to draw statistically better established conclusions, to measure threshold stress intensity factor range (ΔKth) values for base materials and welded joints, and finally, to study the effects of the welding residual stress fields.

Acknowledgements
The presented work was carried out as part of the EFOP- 3.6.1-16-2016-00011 “Younger and Renewing University – Innovative Knowledge City – institutional development of the University of Miskolc aiming at intelligent specialization” project implemented in the framework of the Széchenyi 2020 program. The realization of this project is supported by the European Union, co-financed by the European Social Fund.

References

[1] Allen RJ, Booth GS and Jutla T 1988 Fatigue and Fracture of Engineering Materials and Structures 11/1 45
[2] Allen RJ, Booth GS and Jutla T 1988 Fatigue and Fracture of Engineering Materials and Structures 11/2 71
[3] Ohta A, Maeda Y, Kosuge M, Machida S and Yoshinari H 1989 Transactions of the Japan Welding Society 20/1 17
[4] Merkblatt DVS 2401 Teil 1 Oktober 1982 Bruchmechanische Bewertung von Fehlern in Schweissverbindungen. Grundlagen und Vorgehensweise
[5] Det norske Veritas, Classification Notes, Note No. 30.2 August 1984 Fatigue strength analysis for mobile offshore units
[6] BS 7910 1999 Guide on methods for assessing the acceptability of flaws in fusion welded structures
[7] Merkblatt DVS 2401 Teil 2 April 1989 Bruchmechanische Bewertung von Fehlern in Schweissverbindungen. Praktische Anwendung
[8] Paris P and Erdogan F 1963 Journal of Basic Engineering, Transactions of the ASME 528
[9] Lukács J 1992 Reliability of Cyclic Loaded Welded Joints Having Cracks CSc dissertation (in Hungarian)
[10] Lukács J 2003 Materials Science Forum 414-415 31
[11] Gáspár M, Balogh A and Sas I 2015 Proceedings of IIW 2015 International Conference, Paper IIW 2015 1504 1
[12] Kalácska E, Májlinger K, Fábián ER and Spena PR 2017 Materials Science Forum 885 80
[13] Májlinger K, Kalácska E and Spena PR 2016 Materials Design 109 615

- određivanje kritične veličine prsline koje se može proširiti;
- izračunavanje životnog veka utvrđenog veličinom prsline koja se širi;
- proračun preostalih radnih funkcija, uticaj na vrednosti radnog veka i funkciju radnog veka (drugim rečima, studija parametara);
- pouzdanost procene preostalog radnog veka;
- proračun parametra oštećenja i funkcije oštećenja [25].
Potrebna su dalja ispitivanja kako bi se izvukli statistički bolje utvrđeni zaključci, izmerili vrednosti praga faktora intenziteta napona (ΔKth) za osnovne materijale i zavarene spojeve i, na kraju, da bi se proučio efekat zaostalih polja zaostalih napona usled zavarivanja.

Priznanja
Predstavljeni rad sproveden je u okviru projekta EFOP-3.6.1-16-2016-00011 „Mlađi i obnavljajući univerzitet - Inovativni grad znanja - institucionalni razvoj Univerziteta u Miskolcu sa ciljem inteligentne specijalizacije“ koji se realizuje u okviru Szechenii 2020 program. Realizaciju ovog projekta podržava Evropska unija, a sufinansira ga Evropski socijalni fond.

[14] Gáspár M, Balogh A 2013 Production Processes and Systems 6(1) 9
[15] Dobosy Á, Gáspár M and Jámbor P 2017 3rd Young Welding Professionals International Conference (YPIC2017), Halle (Saale) 1
[16] https://hks-prozesstechnik.de/en/about-hks/ accessed 11 January 2019
[17] ASTM E647-11e1 2011 Standard Test Method for Measurement of Fatigue Crack Growth Rate
[18] Dobosy Á 2017 Design limit curves for high strength steel structures under cyclic loading condition PhD thesis (in Hungarian)
[19] Lukács J 2012 Bányászati és Kohászati Lapok – Bányászat 145 43 (in Hungarian)
[20] Lukács J and Dobosy Á 2017 IIW-DOC XIII-2692-17
[21] Ritchie RO 1979 International Materials Reviews 5-6 205
[22] Taylor D 1985 Compendium of Fatigue Thresholds and Crack Growth Rates EMAS, Warley
[23] Taylor D and Jianchun L (Eds.) 1993 Sourcebook on fatigue crack propagation: threshold and crack closure EMAS, Warley
[24] Farahmand B 2008 Multiscale Fatigue Crack Initiation and Propagation of Engineering Materials: Structural Integrity and Microstructural Worthiness, Solid Mechanics and its Applications 152 Springer, Dordrecht 1
[25] Lukács J 2003 Metal Structures – Design, Fabrication, Economy Millpress, Rotterdam

Muralimohan Cheepua, Jung Hyun Parkb, Hyo Jin Baekc, Sang Myung Chod

Improvement of hot cracking susceptibility and productivity using Super-TIG welding for 9% Nickel-steel

Poboljšanje osetljivosti na vruće prsline i produktivnost upotrebom Super-TIG zavarivanja čelika sa 9% nikla

Originalni naučni rad / Original scientific paper
Rad je u izvornom obliku objavljen u okviru 72. IIW godišnje Skupštine i međunarodne konferencije održane u Bratislavi-Slovačka 07-12. Jula 2019
Rad primljen / Paper received:
Maj 2020.

Adresa autora / Author's address:
Department of Materials System Engineering, Pukyong National University, Busan, Republic of Korea
amuralicheepu@gmail.com, bjungsoug@naver.com, cvitx157@nate.com, dpnwcho@pknu.ac.kr

Ključne reči: Super-TIG zavarivanje, C-dodatni materijal, Vruće prsline, Čelik sa 9% nikla, FCAW

Keywords: Super-TIG Welding, C-Filler, Hot cracking, 9% Nickel steel, FCAW

Abstract

9% Nickel steel has been widely used for storage of liquefied gases, oxygen, and nitrogen in competition with aluminium and austenitic alloys due to its low cost. The development of 9% nickel steel with low ductile-brittle transition temperatures reformed the LNG industry by extensive storage and transportation. In recent years, the demand for 9% nickel steel fuel tanks increasing due to the International Maritime Organization regulations on the reduction of sulphur oxides from 3.5% to 0.5%. Hence, the LNG fuel tanks made with 9% nickel steel became a major part of the international energy industry. However, the weldability, fabrication cost, and productivity of these steels are one of the major concerns for manufacturers. Flux cored arc welding (FCAW) process is the most commonly used joining method for 9% nickel steel with Hastelloy fillers. In FCAW, the loss of deposited metal due to inter pass cleaning by grinding action caused to a reduction in total productivity. Demands for higher production, low cost, better mechanical properties, and reliability are the main driving forces for new developments in this area. To achieve these, the most recently developed “Super-TIG Welding” with C-type filler was successfully applied to improve the 9% Nickel steel weldability, productivity and, mechanical and metallurgical properties of the butt welds. In Super-TIG welding, alloy 625 filler was used, which is cheaper and good weldability over the Hastelloy fillers. The weldability evaluation tests resulted in improved resistance to hot cracking susceptibility using Super-TIG welding. The mechanical properties of the Super-TIG welded joints performed better than the FCAW joints. Most importantly, the productivity of the welding

Rezime

Čelik sa 9% nikla se široko koristi za skladištenje utečnjenih gasova, kiseonika i azota u konkurenciji sa aluminijumom i austenitnim čelicima, zbog niske cene. Razvoj čelika sa 9% nikla sa niskim prelaznim temperaturama duktilno-krto, reformisao je TNG industriju obimnim skladištenjem i transportom. Poslednjih godina povećava se potražnja za rezervoarima za gorivo od čelika sa 9% nikla zbog propisa Međunarodne pomorske organizacije o smanjenju sumpornih oksida sa 3,5% na 0,5%. Stoga su rezervoari za TNG gorivo napravljeni od čelika sa 9% niklap ostali glavni deo međunarodne energetske industrije. Međutim, zavarivanje, trošak izrade i produktivnost ovih čelika predstavljaju jednu od glavnih briga proizvođača. Postupak zavarivanja punjenom žicom (FCAW) je najčešće korišćen način spajanja za čelik sa 9% nikla sa Hastelloy dodatnim materijalima. Kod FCAW, gubitak nanetog metala usled međučišćenja postupkom brušenja, uzrokuje smanjenje ukupne produktivnosti. Potražnja za većom proizvodnjom, niskim troškovima, boljim mehaničkim svojstvima i pouzdanošću su glavne pokretačke snage za nova dostignuća u ovoj oblasti. Da bi se ovo postiglo, nedavno razvijeno „Super-TIG zavarivanje“ sa C-tipom dodatnog materijala,uspešno je primenjeno za poboljšanje zavarivanja, produktivnosti i mehaničkih i metalurških karakteristika zavarivanja čelika sa 9% nikla. Pri Super-TIG zavarivanju korišćen je dodatni materijal od legure 625, što je jeftinije i postiće bolje zavarivanje u odnosu na Hastelloy dodatne materijale. Testovi za ocenjivanje zavarivanja rezultirali su poboljšanom otpornošću na vruće prsline pomoću Super-TIG zavarivanja. Mehaničke osobine Super-TIG zavarenih spojeva su bolje od

dramatically improved by Super-TIG welding. Super-TIG welding is capable of producing higher feeding rates with clean beads. Therefore, the alloy 625 C-Filler and avoidance of inter pass cleaning in Super-TIG welding resulting in increased productivity. The newly developed Super-TIG welding achieved many things to obtain satisfactory products in the recent welding industry.

1. Introduction

In recent years, the demand for liquified petroleum gas (LPG) and liquified natural gas (LNG) is continuously increasing for the avoidance of environmental pollution. There are different types of LNG carriers developed for transportation and storage across the countries. According to the International Maritime Organization (IMO), LNG carriers classified into two types, such as independent and membrane types [1]. The 9% Ni steel was initially developed by the International Nickel Company (INC) in 1942. At the first time, 9% Ni steels had applied to the liquid oxygen tanks in the year of 1952, and then it has been used most commonly for the inner walls of LNG fuel tanks ever since as ferritic grade steel for sub-critical temperature applications [2].

Moreover, 9% Ni steel proved to have enhanced notch toughness at liquid nitrogen temperature and to provide a sturdy welded vessel at -196 ºC without any heat treatment methods after welding. The excellent of high strength and toughness properties obtained due to the alloying addition of 9% Ni as a primary source of steel. These steels mainly used in connection with the transportation and storage of LNG [3]. The fabrication of these steels raised more significant issues to get defect free joints. Even though it is continuously using for the construction of LNG vessels and its demand does not fall because of their excellent fatigue strength and toughness. The steels of 9% Ni is extensive uses in the vessels as an inner wall of the fuel and storage tank owing to the outstanding fracture toughness at the cryogenic environment of -196 ºC [4]. Therefore, the inner wall of the 9% Ni directly contacted with the LNG. The LNG tank constructed only with welded structures. However, the formation of weld defects such as pores, lack of fusion, undercuts, and inclusions can significantly deteriorate the fracture strength of the welded structures. The evaluation of heat affected zone (HAZ) properties of the variety of steels by experimental and simulation methods, impact tests, and metallurgical characterization investigations performed. The identification of the 9% Ni steels

FCAW spojeva. Ono što je najvažnije, produktivnost zavarivanja dramatično je poboljšana Super-TIG zavarivanjem. Super-TIG zavarivanje može stvoriti veće brzine dodavanja sa čistim zavarima. Stoga legura od 625 C-dodatni materijal i izbegavanje međučišćenja kod Super-TIG zavarivanja rezultuje povećanom produktivnošću. Novorazvijeno Super-TIG zavarivanje postiglo je mnoge stvari kako bi dobilo zadovoljavajuće proizvode u sadašnjoj industriji zavarivanja.

1. Uvod

Poslednjih godina potražnja za tečnim naftnim gasom (TNG) i tečnim prirodnim gasom (TPG) kontinuirano raste kako bi se izbeglo zagađenje životne sredine. Postoje različiti tipovi snabdevanja razvijeni za transport i skladištenje TPG širom zemalja. Prema Međunarodnoj pomorskoj organizaciji (IMO), prevoznici za TPG klasifikovani su u dve vrste, kao što su nezavisni i membranski tip [1]. Čelik 9% Ni je inicijalno razvila Međunarodna kompanija nikla (INC) 1942. godine. Prvo se čelik sa 9% Ni nanosio na rezervoare za tečni kiseonik 1952. godine, a zatim se najčešće koristil za unutrašnje zidove rezervoara za gorivo TPG još od feritne klase čelika za primenu na kritičnim temperaturama [2].

Štaviše, pokazalo se da čelik sa 9% Ni ima poboljšanu zareznu žilavost na pri temperaturi tečnog azota i daje čvrst zavareni sud na -196 ° C bez ikakvih metoda termičke obrade nakon zavarivanja. Izvrsna svojstva visoke čvrstoće i žilavosti koja su dobijena legiranjem sa 9% Ni iz primarnog čelika. Ovi čelici uglavnom se koriste u vezi s transportom i skladištenjem TPG [3]. Izrada ovih čelika pokrenula je značajnije probleme da se dobiju spojevi bez grešaka, Iako se kontinuirano koristi za izgradnju posuda za TPG, njegova potražnja ne opada zbog odlične čvrstoće i žilavosti. Čelici od 9% Ni su u širokoj upotrebi u posudama kao unutrašnji zid rezervoara za gorivo i zahvaljujući izuzetnoj žilavosti loma u kriogenom okruženju od -196 ° C [4]. Stoga je unutrašnji zid čelika sa 9% Ni u direktnom kontaktu sa TPG. Rezervoar za TPG je konstruisan samo kao zavarena konstrukcija. Međutim, nastanak oštećenja zavara kao što su pore, nedostatak stapanja, zajeda i uključaka, može značajno pogoršati čvrstoću na lom zavarenih konstrukcija. Sprovedena su procenjivanja svojstava zona pod uticajem toplote raznovrsnih čelika, eksperimentalnim i simulacionim metodama, ispitivanjima udara i metalurškom karakterizacijom. Identifikovano je da čelik sa 9% Ni ima visok nivo udarnih svojstava na niskim temperaturama, što se zahvaljujući finozrnom strukturom nikl-ferita opušta

have a high level of low-temperature notch impact properties, which owes to the fine-grained structure of the nickel-ferrite is relaxed from the embrittled carbide networks. However, the weldability of 9% Ni steel is excellent, when the proper filler materials used for welding. Moreover, this steel is not susceptible to cracking and exhibits the low amount or almost no degradation of weld properties by the influence of heat input during welding. The maximum allowable heat input for manual welding suggested that is about 3 kJ/mm and the range of inter-pass temperature is 100-150 ºC. The cooling rate is a critical factor for these heat treated steels to determine the final microstructure of the weld and HAZ regions. The effect of heat input has many effects on the formation of HAZ toughness and differs widely, which indicates the change in the fine microstructure of the HAZ [5, 6].

Other than these process-related problems, the selection of proper filler material is a crucial factor in obtaining high strength joints without any problems. However, there are no proper filler materials developed for this material. The filler materials are selected based on the base material composition that is similar, but not identical to the substrate composition. The most commonly used welding consumables for welding of 9% Ni steel are high Ni alloys such as the Hastelloy and Inconel materials. Even though the mechanical strength of the filler materials is lower than that of the 9% Ni steel, the fractures are ductile and are same at the cryogenic temperatures; it is due to their full austenitic phase [7]. There are different grades of filler materials are recommended for welding of 9% Ni steel such as flux cored arc welding (FCAW), shielded metal arc welding (SMAW), and gas metal arc welding (GMAW), gas tungsten arc welding (GTAW) and submerged arc welding (SAW). The using of FCAW wires for the welding of LNG tanks which are the made of 9% Ni steel has limitation due to the tight control of welding parameters in a narrow range is needed to avoid the formation of hot cracks. Most of the FCAW wires were producing with Hastelloy, which are usually using for welding of 9% Ni steel.

As per the above discussion, the welding of 9% Ni steels is for the construction of LNG fuel tanks usually welded with Ni-Mo or Ni-Cr filler materials. Because of this, the total cost of the welded structures of 9% Ni steel is high compared to the other materials. Some of the studies recommended to reduce the price of the welded structures using the same composition of filler materials, but using these the control of heat input is challenging. The using of higher heat inputs caused the reduction in iz krtih karbidnih mreža. Međutim, zavarljivost čelika sa 9% Ni je odlična, kada se kpriste odgovarajući dodatni materijali. Štaviše, ovaj čelik nije podložan prslinama i pokazuje malu ili gotovo nikakvu degradaciju svojstava usled unosa toplote tokom zavarivanja. Predloženi maksimalni dozvoljeni unos toplote za ručno zavarivanje je oko 3 kJ / mm, a raspon međuslojne temperature je 100-150 ºC. Brzina hlađenja je kritični faktor za ove termički obrađene čelike za određivanje konačne mikrostrukture šava i ZUT. Učinak unosa toplote ima brojne efekte na žilavosti ZUT i široko se razlikuje, što ukazuje na promenu fine mikrostrukture ZUT [5, 6].

Pored ovih problema koji se tiču postupka, izbor odgovarajućeg dodatnog, presudan je faktor u dobijanju spojeva visoke čvrstoće bez ikakvih problema. Međutim, za ovaj materijal nisu razvijeni odgovarajući dodatni materijali. Dodatni materijali su izabrani na osnovu sastava osnovnog materijala koji je sličan, ali nije identičan sastavu osnove. Najčešće korišćeni dodatni materijal za zavarivanje čelika sa 9% Ni, su legure sa visokim sadržajem Ni kao što su Hastelloy i Inconel. Iako je mehanička čvrstoća dodatnog materijala manja nego kod čelika sa 9% Ni čelika, lomovi su duktilni i isti su na kriogenim temperaturama; to je zbog njihove potpune austenitne faze [7]. Preporučuju se različite vrste dodatnih materijala za zavarivanje čelika sa 9% Ni, kao što su zavarivanje punjenom žicom (FCAW), obloženom elektrodom (SMAW) i elektrolučno zavarivanje u zaštiti gasa (GMAW), zavarivanje netopivom elektrodom od volframa u zaštiti gasa (GTAW) i zavarivanje pod praškom (SAW). Upotreba punjenih žica za FCAW za zavarivanje rezervoara za TPG koji se izrađuju od čelika sa 9% Ni ima ograničenja zbog oskudne kontrole parametara zavarivanja u uskom rasponu, kako bi se izbeglo stvaranje vrućih prslina. Većina FCAW žica se proizvodi od Hastelloya koji se obično koriste za zavarivanje čelika sa 9% Ni.

Prema gornjoj diskusiji, zavarivanje čelika sa 9% Ni namenjeno je za izradu rezervoara za TPG gorivo, obično zavarenih sa Ni-Mo ili Ni-Cr dodatnim materijalima. Zbog toga su ukupni troškovi zavarenih konstrukcija od čelika sa 9% Ni, visoki u poređenju s drugim materijalima. Neke studije preporučuju da se smanje cene zavarenih konstrukcija koristeći isti sastav dodatnih materijala, ali upotrebom ovih materijala, kontrola unosa toplote postaje izazov. Upotreba većih unosa toplote uzrokovala je smanjenje žilavosti metala šava. Može biti povezana sa zadržanom mikrostrukturom austenita u metalu šava. Međutim, kontrola unosa toplote u

the toughness of the weld metal. It may be related to the retained austenite microstructure in the weld metal. However, the control of heat input in the conventional welding process of FCAW and GTAW is difficult due to the higher requirements of deposition rates. To make it easier the control of heat input rate with respect to deposition rate "Super-TIG" welding process has been investigated. Super-TIG welding is a newly developed TIG/GTAW welding process with the using of C-Filler instead of circular filler. The Super-TIG welding was invented in 2013 by Sang-Myung Cho, Super-TIG Welding Co. Ltd. Korea [8-10]. Super-TIG welding applied successfully to various applications such as wire arc additive manufacturing, thick plate welding of Ni-based alloys, stainless steel alloys, pipe welding, overlay clad welds with high deposition and with moderate heat inputs. The feature of Super-TIG welding is high productivity compared to conventional TIG/GTAW welding processes [11].

The present investigation aims to enhance the productivity of the welded structures of 9% Ni steel using Super-TIG welding. In addition to this, the problem of hot cracks in the weld metal minimized with the deposition of clean weld metal and reduction of low-temperature inclusions generation by Super-TIG welding. If Super-TIG welding applied to 9% Ni steel, it could adopt low-cost Inconel filler instead of expensive Hastelloy, which is using for FCAW. Moreover, the productivity of Super-TIG welding determined over the FCAW. The Fisco hot crack tests were conducted to evaluate the hot crack in the Super-TIG and FCAW weld metal. The superior welds without hot cracks and high production rate obtained by using a newly developed process of Super-TIG welding.

2. Experimental Procedure

In the present study, the base material of 9% Ni steel with a thickness of 20 mm used for butt welding and Fisco hot crack tests. The joint design for butt welding prepared with the groove angle of 60º, the width of plates is 300 mm, the root gap between plates is 3 mm, and a length of plates is 600 mm. Fig. 1 shows the butt joint configuration and macrostructure of the final welded joint. The back side of the weld such as root weld was deposited on the groove which was applied a process of air gouging. The joints were made using of Super-TIG welding with a Alloy 625 C-Filler (Super-TIG welding Co. Ltd. Korea) with a shielding gas of Ar+7%H2. The deposition completed for welding within 6 passes on the front side and 2 passes on the backside.

konvencionalnom postupku zavarivanja FCAW i GTAW je teška zbog većih zahteva brzina deponovanja. Da bi se olakšala kontrola brzine unosa toplote u odnosu na brzinu deponovanja, ispitan je „Super-TIG" postupak zavarivanja.Super-TIG zavarivanje je novorazvijeni TIG / GTAW postupak zavarivanja sa korišćenjem C-dodatnog materijala umesto kružnog dodatnog materijala. Zavarivanje Super-TIG izumeo je 2013. Sang-Miung Cho, kompanija Super-TIG Welding Co. Ltd. Korea [8-10]. Super-TIG zavarivanje uspešno se primenjuje u raznim primenama kao što su aditivna proizvodnja elektrolučnim zavarivanjem žicom, debelih ploča od legura na bazi Ni, nehđajućeg čelika, zavarivanje cevi, izardi plakatura sa velikim brzinama deponovanja i sa umerenim unosom toplote. Karakteristika Super-TIG zavarivanja je visoka produktivnost u poređenju sa konvencionalnim postupcima zavarivanja TIG / GTAW [11].

Cilj ovog istraživanja je povećanje produktivnost zavarenih konstrukcija od čelika sa 9% Ni koristeći Super-TIG zavarivanje. Pored toga, problem vrućih prslina u metalu šava, sveden je na minimum problem sa deponovanjem čistog metala šava i smanjenjem stvaranja niskotemperaturnih uključaka. Ako bi se Super-TIG zavarivanje primenjivalo na čelik sa 9% Ni, umesto skupog Hastelloy-a, koji se koristi za FCAW, mogao bi da se koristi jeftiniji Inconel. Štaviše, produktivnost Super-TIG zavarivanja određena je kao veća od FCAW. Srovedeni su Fisco testovi kako bi se procenile vruće prsline u metalu šava izvedenih postupcima Super-TIG i FCAW. Vrhunsko zavarivanje bez vrućih prslina i visoke proizvodne stope dobijene su korišćenjem novorazvijenog postupka zavarivanja Super-TIG.

2. Eksperimentalni postupak

U ovoj studiji, osnovni materijal čelik sa 9% Ni, debljine 20 mm koristi se za sučeono zavarivanje i Fisco test na vruće prsline. Dizajn spojeva za sučeono zavarivanje pripremljen je sa uglom žljeba od 60º, širina ploča je 300 mm, razmak između ploča je 3 mm, a dužina ploča 600 mm. Sl. 1 prikazuje konfiguraciju sučeonog spoja i makrostrukturu konačnog zavarenog spoja. Na konra stranu šava, kao koreni zavar napravljen je žlijeb koji je primijenjen postupkom žljebljenja vazduhom. Spojevi su napravljeni korišćenjem Super-TIG zavarivanja sa legurom 625 C-dodatnim materijalom (Super-TIG zavarivanje Co. Ltd. Koreja) sa zaštitnim gasom Ar + 7% H2. Nanošenje je završeno zavarivanjem u 6 prolaza na prednjoj strani i 2 prolaza na kontra strani.

-Kraj 1. dela NASTAVAK U SLEDEĆEM BROJU

Lina YU[a], Kazuyoshi SAIDA[b], Kazutoshi NISHIMOTO[c]

Extended application of hardness prediction system for temper bead welding of A533B steel to various low-alloy steels

Proširena primena sistema za predviđanje tvrdoće kod zavarivanja čelika A533B za razne niskolegirane čelike

NASTAVAK IZ PREDHODNOG BROJA
2.deo

CONTINUED FROM PREVIOUS ISSUE
Part 2

Fig. 10 *Hardness distribution comparison of 1.5%Ni steel: (a) 1layer-3pass welding and (b) 6layer-21pass welding*
Sl. 10 *Upoređenje raspodele tvrdoće za čelik 1.5%Ni: (a) 1 sloj-3 prolaza i (b) 6 slojeva-21 prolaz*

Fig. 11 Hardness comparison after 1-Layer and 6-Layer welding of 1.5%Ni steel: (a) 1layer-3pass welding and (b) 6layer-21pass welding
Sl. 11 upoređenje tvrdoća posle 1-slojnog i 6-slojnog zavarivanja čelika 1.5%Ni: (a) 1 sloj-3 prolaza i (b) 6 slojeva-21 prolaz

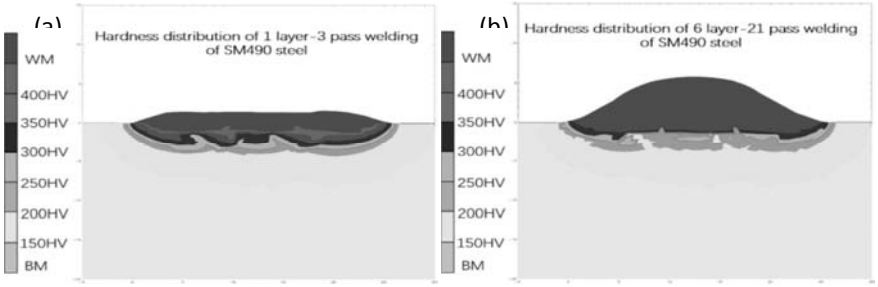

Fig. 12 *Predicted hardness distribution of SM490 steel: (a) 1layer-3pass welding and (b) 6layer-21pass welding*
Sl. 12 *Predviđena raspodela tvrdoća za čelik SM490: (a) 1 sloj-3 prolaza i (b) 6 slojeva -21prolaz*

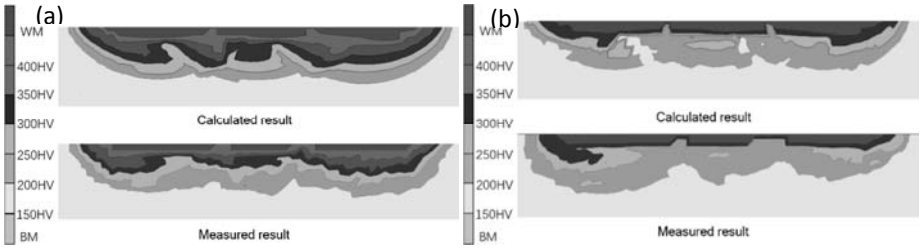

Fig. 13 *Hardness distribution comparison of SM490 steel: (a) 1layer-3pass welding and (b) 6layer-21pass welding*
Sl. 13 *Upoređenje raspodele tvrdoće čelika SM490: (a) 1 sloj-3prolaza i (b) 6 slojeva -21 prolaz*

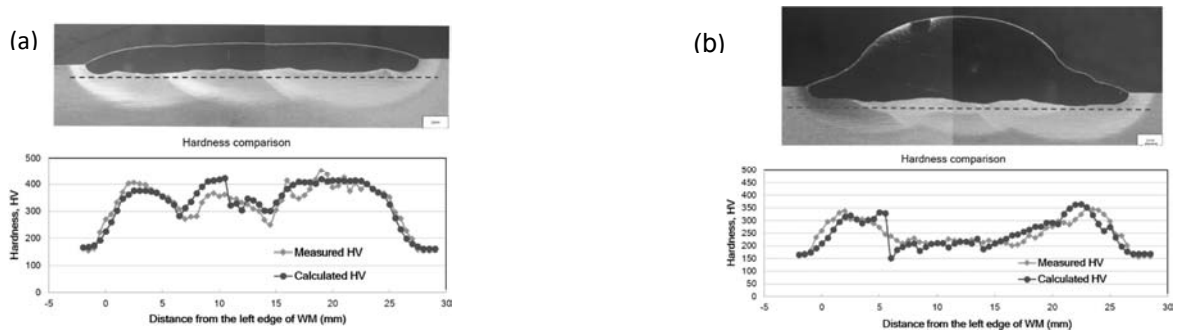

Fig. 14 *Hardness comparison after 1Layer and 6Layer welding of SM490 steel: (a) 1layer-3pass welding and (b) 6layer–21pass welding*
Sl. 14 *Upoređenje tvrdoće posle 1 slojnog i 6 slojnog zavarivanja čelika SM490: (a) 1sloj -3 prolaza i (b) 6 slojeva–21prolaz*

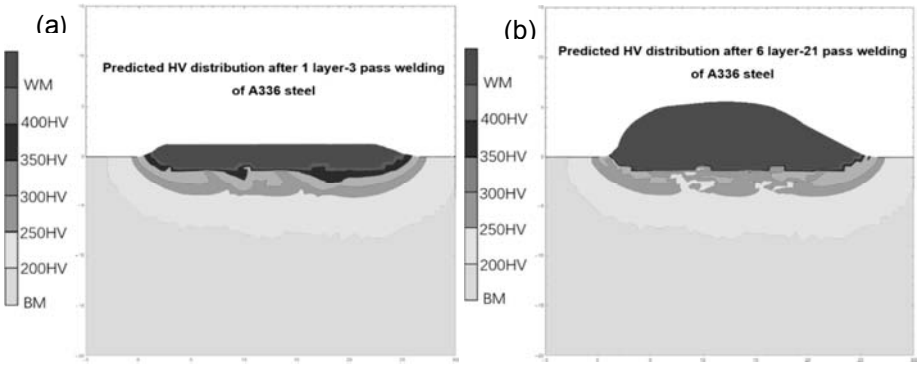

Fig. 15 *Predicted hardness distribution of A336 steel: (a) 1layer-3pass welding and (b) 6layer-21pass welding*
Sl. 15 *Predviđena raspodela tvrdoće kod čelika A336: (a) 1sloj-3 prolaza i (b) 6 slojeva -21 prolaz*

Fig. 16 *Hardness distribution comparison of A336 steel: (a) 1layer-3pass welding and (b) 6layer-21pass welding*
Sl. 16 *Upoređenje raspodele tvrdoće čelika A336: (a) 1 sloj-3 prolaza i (b) 6 slojeva -21 prolaz*

Fig. 17 *Hardness comparison after 1Layer and 6Layer welding of A336 steel: (a) 1layer-3pass welding and (b) 6layer–21pass welding*
Sl. 17 *Upoređenje tvrdoće posle 1 slojnog i 6 slojnog zavarivanja čelika A336: (a) 1 sloj-3 prolaza i (b) 6 slojeva–21 prolaz*

Steel	1-layer	6-layer	Validity
A508	0.92	0.83	○
1.5%Ni	0.91	0.82	○
SM490	0.89	0.81	○
A336	0.55	0.19	×

Table 3. *Correlation coefficient between the predicted hardness and measured hardness*
Tabela 3. *Koeficijent korelacije između predviđene i izmerene tvrdoće*

5. Discussion of the extended hardness prediction method

Fig. 18 illustrates the relationship between hardness after temper and LMP of 5 kinds of steel. It can be found that the hardness of A508, 1.5%Ni, SM490 steels after temper have a good linear relationship with LMP same to the original A533B steel, indicating that A508, 1.5%Ni, SM490 steels are the steels without secondary hardening. However, there is no linear relationship between the hardness of A336 steel and LMP, meaning that A336 steel is the steel with secondary hardening. It follows that the proposed hardness prediction method is useful and effective for estimating the tempering effect in temper bead welding of the low-alloy steels without secondary hardening, expect for the low-alloy steels with secondary hardening.

As shown in Table 3, the correlation coefficient between the predicted hardness and the experimentally measured hardness of A508, 1.5%Ni, SM490 steels also changed from high to low. Based on the microstructure observation at different peak temperatures, the schematic illustration of phase retransformation of 4 kinds of steel can be obtained as illustrated in Fig. 19. When the peak temperature is higher than Ac_3 or lower than Ac_1, both phase composition and grain size are similar for all kinds of steel. However, when the peak temperature is between Ac1 and Ac3, both phase composition and grain size of A508 steel is similar with A533B steel, while there are little different for 1.5%Ni and SM490 steels. This explains the difference of the correlation coefficient of the A508, 1.5%Ni, SM490 steels. But because the temperature range between Ac1 and Ac3 is very narrow, the hardness in the whole HAZ zone have been successfully predicted using the proposed method. Therefore, the hardness of the other low-alloy steels without secondary hardening can be predicted by using the extended hardness database of A533B, from the view of engineering.

Above all, the low-alloy steel has been classified as Group A~D as illustrated in Fig. 20. Group A~C are the low-alloy steels without secondary hardening, while Group D is the low-alloy steels with secondary hardening. For the Group A~C without secondary hardening, the currently proposed extended method is effective for estimating the

5. Diskusija o proširenoj metodi predviđanja tvrdoće

Sl. 18 prikazuje odnos između tvrdoće nakon otpuštanja i LMP kod 5 vrsta čelika. Može se utvrditi da tvrdoća čelika A508, 1,5% Ni, SM490 čelika ima dobru linearnu vezu sa LMP-om isto kao i originalni čelik A533B, što ukazuje da su A508, 1,5% Ni, SM490 čelici bez sekundarnog otvrdnjavanja. Međutim, ne postoji linearni odnos između tvrdoće čelika A336 i LMP, što znači da je čelik A336 čelik sa sekundarnim otvrdnjavanjem. Iz toga sledi da je predložena metoda predviđanja tvrdoće korisna i efikasna za procenu efekta otpuštanja pri zavarivanju zavara za otpuštanje niskolegiranih čelika bez sekundarnog otvrdnjavanja, a očekujemo i kod niskolegiranih čelika sa sekundarnim otvrdnjavanjem.

Kao što je prikazano u Tabeli 3, koeficijent korelacije između predviđene tvrdoće i eksperimentalno izmerene tvrdoće čelika A508, 1,5% Ni, SM490 takođe se menjao od visoke do niske. Na osnovu posmatranja mikrostrukture pri različitim vršnim temperaturama, šematski prikaz fazne retransformacije četiri vrste čelika može se postići kao što je prikazano na slici 19. Kada je vršna temperatura viša od Ac3 ili niža od Ac1, i fazni sastav i veličina zrna slične su za sve vrste čelika. Međutim, kada je vršna temperatura između Ac1 i Ac3, i fazni sastav i veličina zrna čelika A508 su slični čeliku A533B, dok su za čelike 1,5% Ni i SM490 malo različite. Ovo objašnjava razliku koeficijenta korelacije čelika A508, 1,5% Ni, SM490 čelika. Ali budući da je temperaturni opseg između Ac1 i Ac3 vrlo uzak, tvrdoća u celoj ZUT uspešno se predviđa pomoću predložene metode. Stoga se tvrdoća ostalih niskolegiranih čelika bez sekundarnog otvrdnjavanja može predvidjeti upotrebom proširene baze podataka o tvrdoći A533B, sa stanovišta tehnike.

Povrh svega, niskolegirani čelik je klasifikovan kao grupa A-D kao što je prikazano na slici 20. Grupa A-C su niskolegirani čelici bez sekundarnog otvrdnjavanja, dok je grupa D niskolegirani čelici sa sekundarnim otvrdnjavanjem. Za grupu A ~ C bez sekundarnog otvrdnjavanja, trenutno predložena proširena metoda je efikasna za procenu efekta otpuštanja tokom zavarivanja zavara za otpuštanje.

tempering effect during temper bead welding. Thus, the appropriate welding conditions would be able to optimize before the actual welding.

Stoga bi se odgovarajući uslovi zavarivanja mogli optimizirati pre stvarnog zavarivanja.

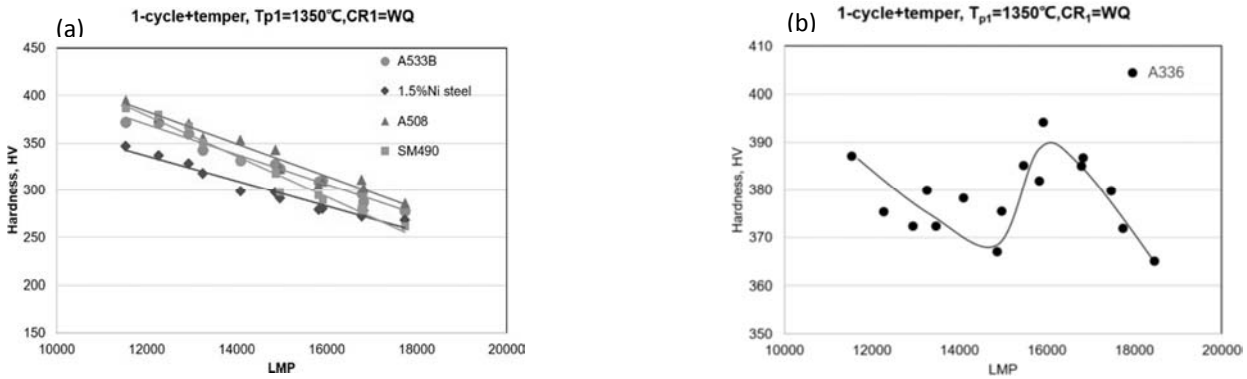

Fig. 18 *Relationship between hardness after temper and LMP of 5 kinds of steels*
Sl. 18 *Međusobni odnos između tvrdoća posle otpuštanja i LMP za 5 vrsta čelika*

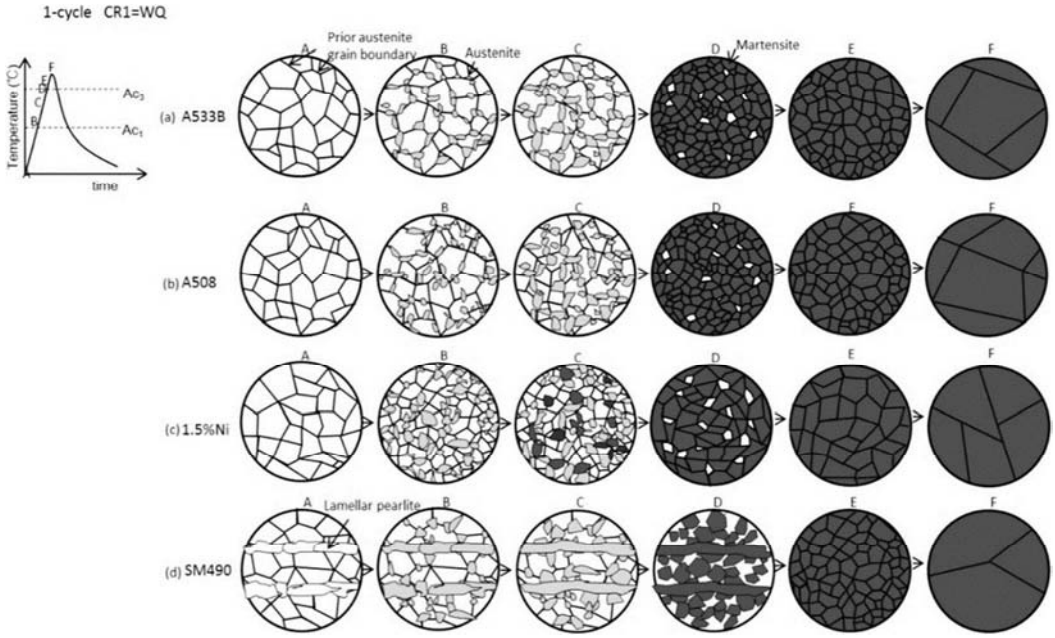

Fig. 19 *Schematic illustration of transformation*
Sl. 19 *Šematska ilustracija transformacije*

6. Conclusions

In the present study, the generalized hardness prediction method applicable for the other low-alloy steels has been conducted by utilizing the presented hardness data-base of A533B steel.

1) Using the proposed extended hardness prediction method, hardness distribution in HAZ of temper bead welding for A508, 1.5%Ni and SM490 steels were calculated based on the thermal cycles simulated by finite element method.

2) The predicted hardness was in good accordance with the experimentally measured result for A508, 1.5%Ni, SM490 steels expect for A336 steel. It followed that the bead welding for the low-alloy steels without secondary hardening.

6. Zaključci

U ovom istraživanju, sprovedena je opšta metoda predviđanja tvrdoće koja se primenjuje za ostale niskolegirane čelike korišćenjem predstavljene baze podataka o tvrdoći A533B čelika.

1) Korišćenjem predložene proširene metode predviđanja tvrdoće, raspodela tvrdoće u ZUT zavara za otpuštanje za čelike A508, 1,5% Ni i SM490 izračunata je na osnovu toplotnih ciklusa simuliranih metodom konačnih elemenata.

2) Predviđena tvrdoća bila je u dobroj usaglašenosti s eksperimentalno izmerenim rezultatom za čelike A508, 1,5% Ni, SM490 a očekuje se i za čelik A336. Iz toga je usledilo zavarivanje zavara kod niskolegiranih čelika bez sekundarnog otvrdnjavanja.

3) Through this method, the hardness of low-alloy steels without secondary hardening could be predicted before the actual welding, thus the appropriate welding conditions would be able to optimize before actual welding, which is very useful for the repair welding for large structures

3) Ovom metodom se može predvideti tvrdoća niskolegiranih čelika bez sekundarnog otvrdnjavanja pre stvarnog zavarivanja, ako bi se odgovarajući uslovi zavarivanja mogli optimizirati pre stvarnog zavarivanja, što je vrlo korisno za reparaturno zavarivanje velikih konstrukcija

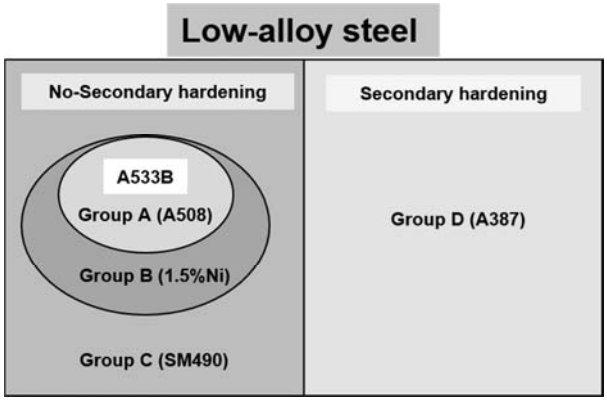

Fig. 20 *Group of low-alloy steel types*
Sl. 20 *Grupa tipova niskolegiranih čelika*

References
Bibliografija

[1] N. Yurioka and Y. Horii, Recent developments in repair welding technologies in Japan, Science and Technology of Welding & Joining, 11 (2006), 255-264.
[2] J. Liao, K. Ikeuchi and F. Matsuda, Toughness Investigation on Simulated Weld HAZs of SQV-2A Pressure Vessel Steel, Nuclear Engineering and Design, 183 (1998), 9-20.
[3] L. Yu, Y. Nakabayashi, M. Sasa, S. Itoh, K. Saida, M. Mochizuki, K. Nishimoto, M. Kameyama, S. Hirano and N. Chigusa, Neural Network Prediction of Hardness in HAZ of Temper Bead Welding using the Proposed Thermal Cycle Tempering Parameter (TCTP), ISIJ International, 51 (2011), 1506-1515.
[4] L. Yu, K. Saida, M. Mochizuki, M. Kameyama, N. Chigusa and K. Nishimoto, Hardness Prediction of HAZ in Temper Bead Welding by Non-Consistent Layer Technique, E-Journal of Advanced Maintenance, 6 (2014), 34-47.
[5] L. Yu, K. Saida, S. Hirano, N. Chigusa, M. Mochizuki, and K. Nishimoto, Application of neural network based hardness prediction method to HAZ of A533B steel produced by laser temper bead welding, Welding in the World, 61(2017), 483- 498.
[6] R. Viswanathan, D. W. Gandy and S. J. Findlan, Temper bead welding of P-Nos. 4 and 5 materials, EPRI TR-111757, EPRI, Palo Alto, CA, USA, December 1998.
[7] L. Yu, M. SaSa, K. Ohnishi, M. Kameyama, S. Hirano, N. Chigusa, T. Sera, K. Saida, M. Mochizuki and K. Nishimoto, Neural Network-Based Toughness Prediction in HAZ of Low- Alloy Steel Produced by Temper Bead Welding Repair Technology, Science and Technology of Welding and Joining, 18 (2013), 120-134.
[8] D. Deng, H. Murakawa and M. Shibahara, Investigations on welding distortion in an asymmetrical curved block by means of numerical simulation technology and experimental method, Computational Materials Science, 48 (2010), 187–194.
[9] D. Casasent and X. Chen, Radial Basis Function Neural Networks for Nonlinear Fisher Discrimination and Neyman- Pearson Classification, Neural Networks, 16 (2003), 529-535.
[10] H. K. D. H. Bhadeshia, R. C. Dimitriu, S. Forsik, J. H. Pak and J. H. Ryu, Performance of neural networks in materials science, Materials Science and Technology, 25-4(2009), 504- 510.
[11] T. Cool, H. K. D. H. Bhadeshia and D. J. C. MacKay, The yield and ultimate tensile strength of steel welds, Materials Science and Engineering A, 223(1997), 186-20 0.

ČASOPIS ZAVARIVANJE I ZAVARENE KONSTRUKCIJE

Cenovnik oglasnog prostora u četiri uzastopna broja 2020

	A4	2/2	1/1	1/2	1/4	1/8
	dimenzije (mm)	2 x 210 x 297	210 x 297	180 x 120	90 x 120	90 x 60
DIN	crno/beli	-	39 000	23 000	16 000	10 000
	kolor	105 000	75 000	-	-	-

- U cene nije uračunat PDV 20%.
- Objavljivanje oglasa u samo jednom broju iznosi 30% od datih cena.
- Reklamni tekstovi: 25 % od cene površine crno/belih oglasa.
- Dostava materijala:
  - za crno-beli film ili CD (Adobe Photoshop / CorelDRAW);
  - za kolor film ili CD (Adobe Photoshop / CorelDRAW);
  - izrada filma sa CD: 10 % od cene angažovanog prostora.
- Na web prezetaciji DUZS-a, (www.duzs.org.rs), na strani Marketing, objavljuje se pregled firmi-oglašivača sa podacima o glavnim grupama proizvoda/usluga i adresom web prezetacije. Svi posetioci naše web prezentacije mogu da posete i web prezentacije oglašivača, preko aktivnih linkova koji se nalaze na ovoj stranici!

INDEKS OGLAŠIVAČA
ADVERTISERS INDEX

WELDING & WELDED STRUCTURES, Quarterly review

Advertising prices for four successive numbers in 2019

	A4	2/2	1/1	1/2	1/4	1/8
	dimensions (mm)	2 x 210 x 297	210 x 297	180 x 120	90 x 120	90 x 60
EUR	black/white	-	840	432	336	240
	colour	2 640	1 680		-	-

- VAT 20% included.
- Advertising in one number only is 35% of the given prices.
- Commercial articles: 30 % of black/white advertising price.
- Print material:
  - for black/white CD (Adobe Photoshop / CorelDRAW)
  - for color CD (Adobe Photoshop / CorelDRAW).
- All the visitors of our web site may be linked to the advertisers' web site.

1. **ČLANARINA DUZS za 2020. godinu** …… **3.500 dinara**

   Članovima DUZS **GRATIS** godišnje izdanje časopisa "ZAVARIVANJE I ZAVARENE KONSTRUKCIJE"

2. **ČASOPIS "ZAVARIVANJE I ZAVARENE KONSTRUKCIJE" - 2020. godina u slobodnoj prodaji** (u cene je uračunat PDV 10%)**:**
   - cena pojedinačnog broja..... ……. 825 dinara
   - godišnja pretplata za 1 komplet brojeva godišnjeg izdanja…… 2.500 dinara
3. **ČASOPIS - stari brojevi** (u cene je uračunat PDV 10%)

   a) u slobodnoj prodaji:
   - cena pojedinačnog broja za 2018. godinu ..... ……..…… 500 dinara
   - cena pojedinačnog broja za prethodne godine……..…….. 250 dinara

   b) beneficirane cene za članove DUZS:
   - cena pojedinačnog broja za 2019. godinu (pouzećem ili preuzimanjem) .....……..…….. 400 dinara
   - cena pojedinačnog broja za prethodne godine (pouzećem ili preuzimanjem) ……..... Gratis
4. **Knjiga Organizacija i ekonomika zavarivačkih radova –** autor: prof. dr Zoran Radojević (uračunat PDV 10%) ……. 1.045 dinara
5. **Zbirke standarda OBEZBEĐENJE KVALITETA U ZAVARIVANJU, komplet 4 toma** 6.750 dinara